Inversion-Based Hysteresis Compensation Using Adaptive Conditional Servocompensator for Nanopositioning Systems

Yasir K. Al-Nadawi
Electrical and Computer Engineering,
Michigan State University,
East Lansing, MI 48824
e-mail: alnadawi@egr.msu.edu

Xiaobo Tan
Electrical and Computer Engineering,
Michigan State University,
East Lansing, MI 48824
e-mail: xbtan@egr.msu.edu

Hassan K. Khalil
Electrical and Computer Engineering,
Michigan State University,
East Lansing, MI 48824
e-mail: khalil@egr.msu.edu

Nanopositioning stages are widely used in high-precision positioning applications. However, they suffer from an intrinsic hysteretic behavior, which deteriorates their tracking performance. This study proposes an adaptive conditional servocompensator (ACS) to compensate the effect of the hysteresis when tracking periodic references. The nanopositioning system is modeled as a linear system cascaded with hysteresis at the input side. The hysteresis is modeled with a modified Prandtl–Ishlinskii (MPI) operator. With an approximate inverse MPI operator placed before the system hysteresis operator, the resulting system takes a semi-affine form. The design of the ACS consists of two stages: first, we design a continuously implemented sliding mode control (SMC) law. The hysteresis inversion error is treated as a matched disturbance, and an analytical bound on the inversion error is used to minimize the conservativeness of the SMC design. The second part of the controller is the ACS. Under mild assumptions, we establish the well-posedness and periodic stability of the closed-loop system. In particular, the solution of the closed-loop error system will converge exponentially to a unique periodic solution in the neighborhood of zero. The efficacy of the proposed controller is verified experimentally on a commercial nanopositioning device under different types of periodic reference inputs, via comparison with multiple inversion-based and inversion-free approaches.
[DOI: 10.1115/1.4052229]

1 Introduction

Micro/nanopositioning stages driven by piezoelectric actuators are widely used in applications with precision requirements, such as atomic force microscopes [1,2], micromanipulators [3,4], ultra-precision grinding operation [5], mechanical nanomanufacturing system for nanomilling [6], high-precision electrochemical etching-based micromachining [7], nanofabrication of materials [8], and investigation of biological systems over scales ranging from single-molecules to whole cells [9,10]. The critical requirement of precision for these applications poses a challenge of dealing with intrinsic nonlinearities like creep and hysteresis of piezoelectric actuators [11]. Particularly, ignoring hysteresis nonlinearity could lead to either poor tracking performance [12] or unstable responses [13]. Therefore, to ensure the desired accuracy, it is needed to compensate such nonlinearities to remove undesired harmonics in the closed-loop system [14].

A number of techniques and methodologies have been developed in the literature for modeling and control of hysteric behavior. Many mathematical models have been developed to depict the hysteresis phenomenon. Examples of these models include Duhem model [15], Maxwell resistive capacitor model [16], Bouc–Wen model [17], Prandtl–Ishlinskii (PI) model [18], and Preisach model [19,20]. One popular approach to design control systems involves the use of inverse hysteresis models in feedforward open-loop scheme to mitigate the effect of the hysteresis [16,20,21].

Despite the reasonable tracking performance achieved using open-loop inverse compensation, it has been shown that it is necessary to ensure system robustness against model uncertainties and external disturbances [22]. Therefore, the inversion-based feedforward control scheme is often combined with a feedback control law to achieve robustness and enhance tracking performance. In that sense, the inversion error is considered as a matched disturbance, and the feedback control is designed to mitigate its effect on the system performance. Many methodologies along this line have been reported in the literature, including, for example, proportional-integral-derivative-based controller [20,23,24], $\mathcal{H}_\infty$ control [25], iterative control [26,27], model reference adaptive inverse control [28], internal model-based servocompensator [29,30], sliding mode control (SMC) [31–34], and hysteretic perturbation estimation [35–38]. A disturbance observer combined with hysteresis inversion is presented in Ref. [39]. The disturbance observer utilizes an internal model-based estimation of the exogenous disturbances, with an assumption that the internal model dynamics have at least an eigenvalue at the origin. Another approach combines the disturbance observer with repetitive control [40], where a low-pass filter is designed to behave approximately as the nominal dynamics. However, for all these inversion-based approaches, the achieved tracking precision will depend mainly on the smallness of the hysteresis inversion error, which is highly dependent on the accuracy of the hysteresis model and its identified parameters.

Another direction in the control of such hysteretic systems is to implement feedback control without explicit hysteresis inversion. For example, an implicit (pseudo) inverse approach with adaptive sliding mode control was introduced in Ref. [41]. In a similar fashion, the authors of Ref. [42] proposed an implicit inverse approach combined with model reference adaptive control.

Yet another class of approaches treats the hysteretic disturbance and other uncertainties as a lumped matched disturbance, which is estimated and compensated accordingly. Examples of work taking this methodology include disturbance observer combined with sliding mode control [43], uncertainty and disturbance estimator [44], active disturbance rejection control [45,46], extended high-gain observer [47], and dynamic inversion based on extended

Contributed by the Dynamic Systems Division of ASME for publication in the Journal of Dynamic Systems, Measurement, and Control. Manuscript received March 21, 2021; final manuscript received August 17, 2021; published online September 15, 2021. Assoc. Editor: Daniel X. B. Chen.

high-gain observer [48,49]. The hysteresis estimation approach does not require necessarily an inverse hysteresis model to be used in the design of the closed-loop control system.

In this paper, we focus on the design of an adaptive conditional servocompensator (ACS) for a class of systems with hysteresis to track periodic references with high precision. We note that tracking periodic references has broad applications for nanopositioners, for example, in atomic force microscopy. The hysteresis is assumed to be modeled by a modified Prandtl–Ishlinskii (MPI) hysteresis operator [50], which outperforms the classical PI operator with its ability to incorporate asymmetric hysteretic behavior. The paper has the following major contributions:

(1) The hysteresis inversion error is analyzed, and an analytical bound on the inversion error is derived and used in the controller design. As observed in experiments, the controller shows that using this analytical bound gives less conservative results as compared to the case when a constant bound is used.
(2) An output feedback controller is designed using adaptive conditional servocompensator by assuming that the residual disturbance due to imperfect hysteresis inversion is composed of a finite number of unknown frequencies. The unmeasured states are estimated by a high-gain observer.
(3) Periodic stability analysis is conducted using contraction mapping arguments by following the stability analysis framework introduced in Ref. [51]. This approach is useful in establishing the periodic stability in a less conservative manner as compared to Lyapunov-based stability arguments under the smallness assumption for the hysteretic inversion perturbation. However, the main challenge is that our closed-loop control system does not fit exactly the system model assumed in Ref. [51] due to the inclusion of nonsmooth terms in our control law. We are able to establish, under mild assumptions, that the closed-loop system solution will converge exponentially to a unique periodic solution when the inversion error is sufficiently small.

The proposed control approach is experimentally evaluated on a commercial piezoelectric nanopositioner. It shows superior precision tracking performance as compared to for other control approaches implemented on the same apparatus. The four competing control approaches used for comparison are sliding mode control [34], single harmonic servocompensator (SHSC) and multiharmonic servocompensator (MHSC) [29], the dynamic inversion based on extended high-gain observer [49], and a classical PI controller without hysteresis inversion.

It is worth pointing out that part of this work included our preliminary results in Ref. [52]. In this paper, we have extended the work to more thorough and in-depth theoretical analysis by establishing the well-posedness and periodic stability results. In addition, we have added more experiments considering sawtooth and van der Pol references to challenge the controller. In addition, we have prepared a comparative study with other control approaches. We have another relevant publication [53], in which we designed an inversion-free adaptive conditional servocompensator. The main difference between Ref. [53] and the current paper is that Ref. [53] does not require an explicit hysteresis inversion. However, Ref. [53] requires a restrictive assumption on the MPI operator, which compromises its generality in representing the asymmetric hysteresis behavior. The approach in Ref. [53] also requires a low-pass filter with a PI operator at its input. One value added in this work as compared to Ref. [53] is that we are able to establish the periodicity of the closed-loop system variables. This could not be achieved in Ref. [53] because of large hysteretic perturbations in the absence of inverse compensation.

The remaining sections are organized as follows. In Sec. 2, the problem formulation, the system model with hysteresis, and the derivation of the analytical bound of the inversion error are presented. Section 3 explains the adaptive conditional compensator design. In Sec. 4, the periodic stability analysis for the closed-loop system with hysteresis perturbation is discussed. Experimental results are given in Sec. 5. Finally, our conclusion is provided in Sec. 6.

2 Problem Formulation

2.1 System Model With Hysteresis Nonlinearity. Consider the following nonaffine system (depicted in Fig. 1) modeled with linear dynamics preceded by hysteresis input nonlinearity

$$\begin{aligned}\dot{x}(t) &= F_p(x(t)) + B_p u_o(t)\\ y(t) &= x_1(t)\end{aligned} \tag{1}$$

where $x \in \mathcal{R}^n$ is the state vector, y is the measured output, and $u_o \in \mathcal{R}$ is the output of the hysteresis operator

$$u_o(t) = F_h[\nu(\cdot);\varsigma_o](t) \tag{2}$$

where F_h denotes the hysteresis operator, $\nu \in \mathcal{R}$ is the system input, and ς_o represents the initial memory of the hysteresis (we will elaborate more on the hysteresis model in Sec. 2.2). The function F_p and the vector B_p represent the controller canonical form of the linear dynamics

$$F_p = \begin{bmatrix} x_2\\ x_3\\ \vdots\\ x_n\\ f_n(x)\end{bmatrix}_{n\times 1}, \quad B_p = \begin{bmatrix} 0\\ 0\\ \vdots\\ \vdots\\ b\end{bmatrix}_{n\times 1} \tag{3}$$

where $f_n(x) = -a_1x_1 - a_2x_2 - \cdots - a_nx_n$, a_i's and $b > 0$ are the system parameters. The objective is to make the system output $y(t)$ track a desired reference input $y_d(t)$, which is assumed to obey the following assumption.

Assumption 1. *The desired reference y_d and its time-derivatives up to order n are piecewise continuous in t, bounded for all $t \geq 0$, and T-periodic (i.e., $y_d(t) = y_d(t+T)$) for some $T \geq 0$.*

The tracking error is defined as

$$e_1(t) = y(t) - y_d(t)$$

Using the above equation, we can obtain the error dynamics as follows:

$$\dot{e}(t) = F_p(e(t)) + B_p u_o(t) + B_d\delta_d(t) \tag{4}$$

where F_p is defined as in Eq. (3) with argument e instead of x, $e = [e_1, e_2, \ldots, e_n]^T$, $e_i = (\mathrm{d}^{i-1}e)/\mathrm{d}t^{i-1}$ for $i = 2, \ldots, n$, $(\cdot)^T$ denotes the transpose, $B_d = [0, \ldots, 0, 1]^T$, and δ_d is defined as

$$\delta_d(t) = -a_1y_d - a_2\dot{y}_d - \cdots - a_{n-1}y_d^{n-1} - a_ny_d^n$$

Remark 1. The system model (1)–(3) could be generalized to have stable internal dynamics similar to the model formulation in Ref. [54]. The analysis and controller design in the Secs. 3 and 4 could be replicated with the added internal dynamics to reach similar theoretical results.

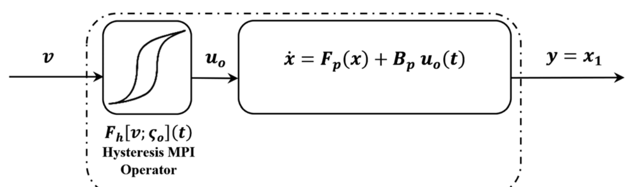

Fig. 1 Schematic of the class of systems considered, with linear dynamics proceeded by a hysteresis operator

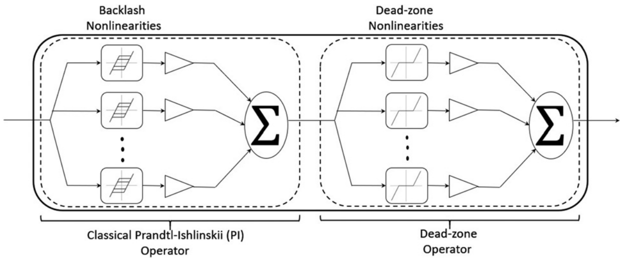

Fig. 2 Block diagram of the finite-dimensional MPI hysteresis operator

2.2 Modified Prandtl–Ishlinskii Hysteresis Operator. To model the hysteresis operator F_h in Eq. (2), we use the MPI operator (illustrated in Fig. 2). This model was originally proposed by Kuhnen [50] in 2003 by combining the classical PI hysteresis operator with another operator represented by a weighted superposition of one-sided deadzone nonlinearities. This modification makes the MPI operator capable of modeling asymmetric hysteretic characteristics as compared to the classical PI operator. The PI operator is a weighted superposition of basic hysteresis units, each of which is modeled with a backlash operator with a threshold r_{th}. The backlash operator for a continuous and monotone input $v(t)$ for $t \in [0, T]$ is given as

$$u_{\text{bk}}(t) = \max\{\min\{v(t) + r_{\text{th}}, u_{\text{bk}}(0)\}, u_{\text{in}}(t) - r_{\text{th}}\} \tag{5}$$

where u_{bk} is the output of the backlash operator, and $u_{\text{bk}}(0)$ is the initial state. In essence, the PI operator consists of weighted integral of a continuum of backlash operators, which makes it an infinite-dimensional operator [55]. Due to practical consideration, a finite-dimensional PI operator is often considered, which is represented by a weighted sum of a finite number of backlash operators. Accordingly, the following assumption is made for the MPI operator.

Assumption 2. *The hysteresis nonlinearity F_h is modeled with a finite-dimensional MPI operator, which consists of $(q+1)$ backlash operators and $(2l+1)$ one-sided deadzone operators, where q and $l \in \mathcal{N}^+$.*

Based on Assumption 2, the output u_b of the PI operator F_b under the input v is given by

$$u_b(t) = F_b[v; x_b(0)](t) = \sum_{i=0}^{q} \theta_{bi} x_{bi}(t) \tag{6}$$

where $x_{bi}(t)$ represents the output of the ith backlash operator such that

$$x_{bi}(t) = \mathcal{P}_{bi}[v; x_{bi}(0)](t) \tag{7}$$

in which $x_{bi}(0)$ is the initial state, and $\theta_{bi} \geq 0$ is the weight of the ith backlash operator. Let $\theta_b = [\theta_{b0}, \theta_{b1}, \ldots, \theta_{bq}]$ be the weight vector and $r = [r_0, r_1, \ldots, r_q]$ be the backlash threshold vector, where $r_0 = 0$ and $r_i \geq 0$ for $i = 1, 2, \ldots, q$. Define the following vectors:

$$\mathcal{P}_b := [\mathcal{P}_{b0}, \mathcal{P}_{b1}, \ldots, \mathcal{P}_{bq}]^T \tag{8}$$

$$x_b := [x_{b0}, x_{b1}, \ldots, x_{bq}]^T \tag{9}$$

$$x_b(0) := [x_{b0}(0), x_{b1}(0), \ldots, x_{bq}(0)]^T \tag{10}$$

By using Eqs. (8)–(10), we rewrite Eq. (6) in a compact form as follows:

$$u_b(t) = \theta_b^T x_b = \theta_b^T \mathcal{P}_b[v; x_b(0)]$$

As mentioned above, the deadzone operator contains a weighted superposition of one-sided deadzone functions. For each one-sided deadzone function $\mathcal{P}_{di}$ with input $u_b(t)$ and a threshold d_i, the output is given as

$$\mathcal{P}_{di}(u_b(t)) = \begin{cases} \max\{u_b(t) - d_i, 0\} & \text{if } d_i > 0 \\ u_b(t) & \text{if } d_i = 0 \\ \min\{u_b(t) - d_i, 0\} & \text{if } d_i < 0 \end{cases} \tag{11}$$

Let $d := [d_{-l}, \ldots, d_0, d_1, \ldots, d_l]^T$ and $\theta_d := [\theta_{d-l}, \ldots, \theta_{d0}, \theta_{d1}, \ldots, \theta_{dl}]^T$ be the deadzone operator thresholds and weights vectors, respectively. Define the deadzone operator vector $\mathcal{P}_d := [\mathcal{P}_{d-l}, \ldots, \mathcal{P}_{d0}, \mathcal{P}_{d1}, \ldots, \mathcal{P}_{dl}]^T$. The output $u_o(t)$ of the MPI operator F_h under the input $v(t)$ with an initial condition state $x_b(0)$ will be

$$\begin{aligned} u_o(t) = F_h[v; x_b(0)](t) &:= \sum_{i=l}^{l} \theta_{di} \mathcal{P}_{di}\left(\sum_{j=0}^{q} \theta_{bj} \mathcal{P}_{bj}[v; x_b(0)](t)\right) \\ &= \theta_d^T \mathcal{P}_d(\theta_b^T x_b(t)) \end{aligned} \tag{12}$$

Let $\mathbb{W}_t^{1,1}$ be the Banach space of the absolutely continuous function $u : [0, t] \to \mathcal{R}$ equipped with a standard norm $||\cdot||_{\mathbb{W}_t^{1,1}}$, which is a combination of the $\mathbb{1}$-norm of the function u and the 1-norm of the first-order time-derivative of u

$$||u||_{\mathbb{W}_t^{1,1}} = ||u||_1 + \int_0^t ||u'(\tau)||_1 d\tau \tag{13}$$

where $u'(\tau))$ is the derivative of u with respect to τ. In Proposition 1, we establish the local Lipschitz property for the MPI operator F_h for any input $u \in \mathbb{W}_L^{1,1} \subset \mathbb{W}_t^{1,1}$ where

$$\mathbb{W}_L^{1,1} = \{u | u : \mathcal{R}_+ \to \mathcal{R}, u|_{[0,t]} \in \mathbb{W}_t^{1,1}, \forall t \geq 0\} \tag{14}$$

Proposition 1. *The MPI operator F_h is locally Lipschitz continuous with constant $L_h = \sum_{-l}^{l} |\theta_{di}| \sum_{j=0}^{q} |\theta_{bj}|$ in the following sense:*

$$\begin{aligned} &\sup_{\tau \in \mathcal{R}_+} ||F_h[u_1; x_b(0)](\tau) - F_h[u_2; x_b(0)](\tau)||_{\mathbb{W}_\tau^{1,1}} \\ &\qquad \leq L_h \sup_{\tau \in \mathcal{R}_+} ||u_1(\tau) - u_2(\tau)||_{\mathbb{W}_\tau^{1,1}} \end{aligned} \tag{15}$$

where u_1, u_2 are two different inputs in the set $\mathbb{W}_L^{1,1}$.

Proof. Consider the PI operator F_b in Eq. (6), under inputs u_1, u_2, and the initial condition $x_b(0)$. By utilizing the Lipschitz continuity property of the PI operator F_b inside $\mathbb{W}_L^{1,1}$ [28,56], one can derive the following inequality:

$$\begin{aligned} &\sup_{\tau \in \mathcal{R}_+} ||F_b[u_1; x_b(0)](\tau) - F_b[u_2; x_b(0)](\tau)||_{\mathbb{W}_\tau^{1,1}} \\ &\quad \leq \sum_{i=0}^{q} |\theta_{b_i}| \sup_{\tau \in \mathcal{R}_+} ||u_1(\tau) - u_2(\tau)||_{\mathbb{W}_\tau^{1,1}} \end{aligned} \tag{16}$$

Similarly, utilizing the Lipschitz continuity property of the deadzone operator P_d (11), we can show

$$\begin{aligned} &\sup_{\tau \in \mathcal{R}_+} ||F_h(F_b[u_1; x_b(0)](\tau)) - F_h(F_b[u_2; x_b(0)](\tau))||_{\mathbb{W}_\tau^{1,1}} \\ &\leq \sum_{i=-l}^{l} |\theta_{di}| \sup_{\tau \in \mathcal{R}_+} ||F_b[u_1; x_b(0)](\tau) - F_b[u_2; x_b(0)](\tau)||_{\mathbb{W}_\tau^{1,1}} \end{aligned} \tag{17}$$

By combining the two inequalities (16) and (17), we get Eq. (15). ∎

2.3 Inversion of the Modified Prandtl–Ishlinskii Operator. As shown in Fig. 3, the hysteresis inversion is achieved by cascading an inverse MPI operator with the MPI hysteresis operator F_h.

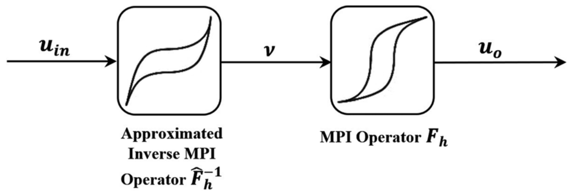

Fig. 3 The feedforward hysteresis inversion

Let $\hat{F}_h$ denotes the approximated forward MPI operator resulted from the model identification.

Assumption 3. *For the MPI operator (12), only the values of the radii vector r and the thresholds vector d are known.*

This assumption is common, and it has been used frequently in the literature (for example, see Refs. [50,57], and [58]). The assumption also implies that the exact values of the PI operator's weight vector θ_b and the deadzone operator's weight vector θ_d are not known. To accommodate that, let $\hat{\theta}_b$ and $\hat{\theta}_d$ be offline identified (approximate) values of the weight vectors θ_b and θ_d, respectively. We denote the errors of these weight vectors as follows:

$$\begin{aligned}\Delta_b &= \theta_b - \hat{\theta}_b \\ \Delta_d &= \theta_d - \hat{\theta}_d\end{aligned} \tag{18}$$

where $\Delta_b \in \mathcal{R}^{q+1}$ and $\Delta_d \in \mathcal{R}^{2l+1}$ are the weight error vectors of the weight vectors θ_b and θ_d, respectively. Consider Fig. 3, and let F_h^{-1} denote the inverse hysteresis operator and $\nu(t)$ represent the generated output of the operator F_h^{-1}. The inverse operator F_h^{-1} is also an MPI operator, and it is defined as

$$\begin{aligned}\nu(t) &= F_h^{-1}[u_{\text{in}}; \bar{x}_b(0)](t) \\ &:= \sum_{i=0}^{q} \bar{\theta}_{bi} \bar{\mathcal{P}}_{bi} \left[\sum_{j=l}^{l} \bar{\theta}_{dji} \bar{\mathcal{P}}_{dj}(u_{\text{in}}(t)); \bar{x}_{bi}(0) \right](t) \\ &= \bar{\theta}_b^T \bar{\mathcal{P}}_b [\bar{\theta}_d^T \bar{\mathcal{P}}_d (u_{\text{in}}(t)); \bar{x}_b(0)](t)\end{aligned} \tag{19}$$

where $\bar{P}_{bi}$ and $\bar{P}_{di}$ are the individual inverse PI and deadzone opertaors, respectively, and $\bar{P}_b = [\bar{P}_{b0}, \ldots, \bar{P}_{bq}]^T$ and $\bar{P}_d = [\bar{P}_{d-l}, \ldots, \bar{P}_{d-1}, \bar{P}_{d0}, \ldots, \bar{P}_{d1}, \ldots, \bar{P}_{dl}]^T$ are the vectors of the inverse PI operator and inverse deadzone operator vectors, respectively. The variables $\bar{x}_b = [\bar{x}_{b0}, \bar{x}_{b1}, \ldots, \bar{x}_{bq}]^T$ and $\bar{x}_b(0) = [\bar{x}_{b0}(0), \bar{x}_{b1}(0), \ldots, \bar{x}_{bq}(0)]^T$ are the vectors of the inverse PI operator state and its initial state, respectively. And $\bar{\theta}_{bi}$ and $\bar{\theta}_{dj}$ are the weights for the individual inverse backlash and deadzone operators, respectively, where $\bar{\theta}_b = [\bar{\theta}_{b0}, \bar{\theta}_{b1}, \ldots, \bar{\theta}_{bq}]^T$ and $\bar{\theta}_d = [\bar{\theta}_{d-l}, \ldots, \bar{\theta}_{d1}, \bar{\theta}_{d0}, \bar{\theta}_{d1}, \ldots, \bar{\theta}_{dl}]^T$. Let $\bar{r} = [\bar{r}_0, \bar{r}_1, \ldots, \bar{r}_q]^T$ and $\bar{d} = [\bar{d}_{-l}, \ldots, \bar{d}_{-1}, \bar{d}_0, \bar{d}_1, \ldots, \bar{d}_l]^T$ be the thresholds vectors of the inverse PI operator and inverse deadzone operator, respectively.

Remark 2. Due to space limitation, the procedure of how to calculate the inverse MPI operators parameters' vectors $\bar{\theta}_b$, $\bar{\theta}_d$, $\bar{r}$, and $\bar{d}$ has been omitted. For more details about these calculations, the readers may consult Ref. [50].

In the subsequent steps, we show that, under sufficiently accurate estimation of the MPI operator weights (θ_b and θ_d), we can make the inversion error arbitrarily small. Moreover, we drive an analytical bound on the hysteresis inversion error, which will be used later to design the controller. Let δ_{inv} denotes the hysteresis perturbation due to imperfect inversion, which can be expressed as

$$\delta_{\text{inv}}(t) = u_o(t) - u_{\text{in}}(t) \tag{20}$$

The approximated MPI hysteresis operator can be expressed as

$$\hat{F}_h = \hat{\theta}_d^T \mathcal{P}_d (\hat{\theta}_b^T \mathcal{P}_b [\nu; x_b(0)]) \tag{21}$$

Using Eq. (21) and by rewriting $u_{\text{in}} = \hat{F}_h[\hat{F}_h^{-1}[u_{\text{in}}; \bar{x}_b(0)]; x_b(0)]$, one can rewrite Eq. (20) as

$$\begin{aligned}\delta_{\text{inv}} &= \mathcal{I}_{\text{inv}}[u_{\text{in}}; x_b(0)](t) \\ &= \theta_d^T \mathcal{P}_d(\theta_b^T x_b(t)) - \hat{\theta}_d^T \mathcal{P}_d(\hat{\theta}_b^T x_b(t))\end{aligned} \tag{22}$$

where $\mathcal{I}_{\text{inv}}$ denotes the operator resulted from the inversion process. In the following proposition, we will show that the output δ_{inv} of the operator $\mathcal{I}_{\text{inv}}$ obeys a growth condition, whose upper bound is a linear function of the input u_{in}, and it can be used later to design a less conservative controller as compared to the case when the inversion error is bounded by a constant such that $|\delta_{\text{inv}}| \leq k_\delta$, where k_δ is some positive constant.

Proposition 2. *Under Assumption 3, if the operator $\mathcal{I}_{\text{inv}}$ is modeled as in Eq. (22), then its output $\delta_{\text{inv}}(t)$ will satisfy the following condition:*

$$|\delta_{\text{inv}}| \leq \Delta_0 |u_{\text{in}}(t)| + \Delta_1 \tag{23}$$

where the constants Δ_0 and Δ_1 can be calculated from the following formulas:

$$\Delta_0 = \varepsilon_{h_{\max}}(||\hat{\theta}_b||_\infty + ||\hat{\theta}_d||_\infty)\left(\left[\sum_{i=0}^{q} |\bar{\theta}_{bi}|\right]\left[\sum_{j=-l}^{l} |\bar{\theta}_{dj}|\right]\right) \tag{24}$$

$$\Delta_1 = \varepsilon_{h_{\max}}(||\hat{\theta}_b||_\infty + ||\hat{\theta}_d||_\infty)\left(\left[\sum_{i=0}^{q} |\bar{\theta}_{bi}|\right] ||\bar{r}||_\infty + ||r||_\infty\right) \tag{25}$$

where $\varepsilon_{h_{\max}} = (q+1)(2l+1)\max(||\Delta_b||_\infty, ||\Delta_b||_\infty)$ is the maximum perturbation of the weight vectors, and $||\cdot||_\infty$ is the infinity norm.

Proof. The backlash operator $\mathcal{P}_{bi}$ with threshold r_i can be represented using the stop operator by the following formula [59]:

$$\mathcal{P}_{si}[\nu(t); x_{bi}(0)](t) = \nu(t) - \mathcal{P}_{bi}[\nu(t); x_{bi}(0)](t) \tag{26}$$

where $\mathcal{P}_{si}$ is the stop operator with threshold r_i. As shown in Fig. 4, the stop operator is bounded from above by its threshold r_i such that

$$|\mathcal{P}_{si}[\nu(t); x_{bi}(0)](t)| \leq r_i \tag{27}$$

Therefore, using Eq. (27), we can show that

$$|\mathcal{P}_{bi}[\nu(t); x_{bi}(0)](t) - \nu(t)| \leq r_i \tag{28}$$

From the Lipschitz property of the deadzone nonlinearity, we can show that $\mathcal{P}_{di}$ satisfies the following inequality:

$$|\mathcal{P}_{di}(\nu_1(t)) - \mathcal{P}_{di}(\nu_2(t))| \leq |\nu_1(t) - \nu_2(t)| \tag{29}$$

Considering Eq. (22), by adding and subtracting the term $(\hat{\theta}_d^T \mathcal{P}_d(\theta_b^T \mathcal{P}_b[\nu(t); x_b(0)](t)))$ and by using Eq. (18), we can rewrite Eq. (22) as follows:

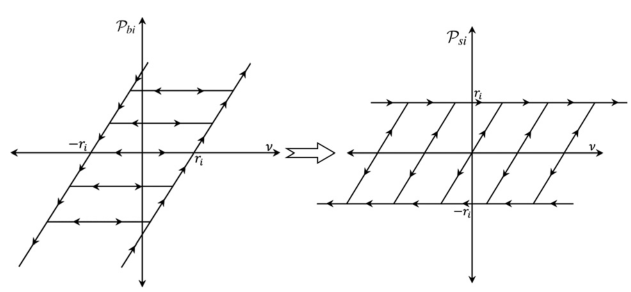

Fig. 4 Characteristics of the backlash operator $\mathcal{P}_{bi}$ as compared to the stop operator $\mathcal{P}_{si}$

$$\delta_{\text{inv}} = \Delta_d^T \mathcal{P}_d(\theta_b^T \mathcal{P}_b[\nu; x_b(0)](t)) + \hat{\theta}_d^T [\mathcal{P}_d(\theta_b^T \mathcal{P}_b[\nu; x_b(0)](t)) - \mathcal{P}_d(\hat{\theta}_b^T \mathcal{P}_b[\nu; x_b(0)](t))] \tag{30}$$

By taking the absolute value of both sides of the above equation, using inequalities (28) and (29), and applying the *Hölder's* inequality, one can get

$$|\delta_{\text{inv}}| \leq \varepsilon_{h_{\max}}(\nu(t) + ||r||_\infty)(||\hat{\theta}_b||_\infty + ||\hat{\theta}_d||_\infty) \tag{31}$$

By taking the absolute value of Eq. (19), we get

$$\nu(t) \leq \left[\sum_{i=0}^{q} |\bar{\theta}_{bi}|\right] \left(\left[\sum_{j=-l}^{l} |\bar{\theta}_{di}|\right] |u_{\text{in}}(t)| + ||\bar{r}||_\infty \right) \tag{32}$$

Finally, by inserting Eq. (32) back into Eq. (31) and arranging the terms, we can obtain Eq. (23). ■

The smallness of the inversion error bound depends directly on the maximum perturbation $\varepsilon_{h_{\max}}$, which depends on how accurate the MPI hysteresis model is. Therefore, the following assumption is made to characterize the smallness of the inversion error in the closed-loop system.

Assumption 4. *There exists a small positive constant $\varepsilon_h \leq \varepsilon_{h_{\max}}$ such that the inversion error (22) can be rewritten in the following form:*

$$\delta_{\text{inv}} = \mathcal{I}_b[u_{\text{in}}; x_b(0)](t) = \varepsilon_h W_{\text{in}}(t) \tag{33}$$

where $W_{\text{in}}(t) = \mathcal{W}_{\text{inv}}[u_{\text{in}}; W_{\text{in}}(0)](t)$, and the hysteresis operator $\mathcal{W}_{\text{inv}}$ is the composite MPI operator due to the inversion.

3 Adaptive Output Feedback Controller Design

3.1 Continuously Implemented Sliding Mode Control Law Design. By using Eq. (20), we can convert the nonaffine hysteretic error system (4) into the following semi-affine system:

$$\dot{e}(t) = F_p(e(t)) + B_p(u_{\text{in}}(t) + \delta_{\text{inv}}(t)) + B_d\delta_d(t) \tag{34}$$

where the semi-affine system means that the system has input u_{in} appears linearly and the perturbation (inversion error δ_{inv}) is modeled with a nonlinear function of the input u_{in} as in Eq. (22). The first step in designing the controller is to design a continuously implemented sliding mode control law. The following surface function is considered:

$$\xi_c = k_1 e_1 + k_2 e_2 + \cdots + k_{n-1}e_{n-1} + e_n \tag{35}$$

where the coefficients $k_1, k_2, \ldots, k_{n-1}$ are positive and chosen to make the following polynomial:

$$\lambda^n + k_{n-1}\lambda^{n-1} + \cdots + k_1$$

Hurwitz. For design purposes, the control input u_{in} is partitioned into two parts; the first part is the equivalent control u_q and the second part is the switching control u_w

$$u_{\text{in}} = u_q + u_w \tag{36}$$

Let $V_c = (1/2)\xi^2$ be used as a Lyapunov function candidate. By using the control law (36) and calculating the time-derivative of the Lyapunov function V_c, the equivalent control u_q is designed as

$$u_q(t,e) = \frac{1}{b}\left[-f_n(e) - \delta_e(e) - \delta_d(t)\right] \tag{37}$$

where $f_n(e) = -a_1e_1 - a_2e_2 - \cdots - a_ne_n$ and $\delta_e(e) = k_1e_2 + \cdots + k_{n-1}e_n$.

Let the switching control law u_w be

$$u_w = -\beta_w(t,e)\text{sat}\left(\frac{\xi_c}{\mu}\right) \tag{38}$$

where β_w is the switching gain function, which will be designed shortly, sat$(\cdot)$ is a standard saturation function, which is defined as follows [60]:

$$\text{sat}(v) = \begin{cases} v, & \text{if } |v| \leq 1 \\ \text{sign}(v), & \text{if } |v| > 1 \end{cases} \tag{39}$$

The parameter $\mu > 0$ is chosen small. To design the switching function β_w, consider the error bound inequality (23). By substituting the desired control law (36) back into the inequality (23), we get

$$\begin{aligned} |\delta_{\text{inv}}| &\leq \Delta_1 + \Delta_0|u_w(t,e) + u_q(t,e)| \\ &\leq \Delta_1 + \Delta_0|u_w(t,e)| + \Delta_0|u_q(t,e)| \end{aligned} \tag{40}$$

Assuming $\Delta_0 < 1$, the switching function is designed as

$$\beta_w(t,e) = \Gamma_1\left[\frac{\Delta_1 + \Delta_0|u_q(t,e)|}{1-\Delta_0} + \Gamma_0\right] \tag{41}$$

where $\Gamma_0 > 0$ and $\Gamma_1 > 1$ are controller parameters. Inserting the control laws (36) and (37), and utilizing the error bound inequality (40), we get

$$\dot{V}_c < -b[(\Delta_1 + \Delta_0|u_q(t,e)|)(\Gamma_1 - 1) + \Gamma_0\Gamma_1]|\xi_c|$$

then the control law (36) achieves a nonzero steady-state error. In other words, if μ is chosen small enough, the closed-loop system trajectory will reach the boundary layer $\{|\xi_c| \leq \mu\}$ and will stay in for all future time. The purpose of using the saturation function instead of the signum function in the switching control law (38) is to avoid the chattering of the control action; however, the drawback is that the error e will be $\mathcal{O}(\mu)$ instead of zero. To mitigate the residual error, we use the adaptive conditional servomechanism [54,61], which will be discussed in Sec. 3.2.

For the output feedback case, we assume that only e_1 is available for measurement. Therefore, to reconstruct the unmeasured states, we design a high-gain observer with the following structure:

$$\dot{\hat{e}}(t) = \hat{f}_o(e) + \hat{g}_o(e_1 - \hat{e}_1) \tag{42}$$

where

$$\hat{f}_o = \begin{bmatrix} \hat{e}_2 \\ \hat{e}_3 \\ \vdots \\ \hat{e}_n \\ 0 \end{bmatrix}_{n\times 1}, \quad \hat{g}_o = \begin{bmatrix} \frac{h_1}{\varepsilon} \\ \frac{h_2}{\varepsilon^2} \\ \vdots \\ \frac{h_n}{\varepsilon^n} \end{bmatrix}_{n\times 1}$$

where $\hat{e}_i$ is the estimated state of e_i, ε is a very small positive design parameter, and h_i is the estimation gain for the ith state, where the gains are chosen such that the polynomial $\lambda^n + h_1\lambda^{n-1} + \cdots + h_{n-1}\lambda + h_n$ is Hurwitz. Accordingly, the desired control law u_{in} (36) and the surface function ξ_c (35) are modified by replacing e with $\hat{e}$.

In order to avoid the effect of observer peaking, the observer states are saturated before being plugged into the control law. This remedy, suggested in Ref. [62], will make the control law globally bounded in its arguments in the domain of interest.

3.2 Adaptive Conditional Servocompensator Design. In the boundary-layer phase, due to the hysteresis inversion error, there is a nonvanishing matched perturbation δ_{inv}. In theory, the disturbance $\delta_{\text{inv}}(t)$ could contain an infinite number of harmonics of the reference signal frequency y_d. However, for practical reasons and based on the adaptive conditional servomechanism theory [54,61], we will assume a finite number of frequencies to be estimated by the conditional servocompensator. In particular, the spectra of tracking errors in our experiments (see Sec. 5) are well approximated by a few harmonic elements, providing support for the assumption below.

Assumption 5. *The hysteresis inversion error $\delta_{\text{inv}}(t)$ is generated by an exogenous neutrally stable linear dynamical system*

$$\begin{aligned}\dot{\omega} &= S\omega \\ \delta_{\text{inv}}(t) &= \Gamma\omega\end{aligned} \tag{43}$$

where $\omega \in \varkappa \subset \mathcal{R}^m$ is the state vector of the exosystem, $\varkappa$ is a compact set, and the matrices S and Γ are given by

$$S = \begin{bmatrix} 0 & 1 & 0 & \dots & 0 \\ 0 & 0 & 1 & \dots & 0 \\ \vdots & & & & \vdots \\ 0 & \dots & \dots & 0 & 1 \\ c_0 & c_1 & \dots & \dots & c_{m-1} \end{bmatrix}_{m\times m}$$

$$\Gamma = [1 \quad 0 \quad \dots \quad \dots \quad 0]_{1\times m}$$

The above assumption means that the disturbance δ_{inv} is a linear combination of constant and sinusoidal components. The word "conditional" in conditional servocompensator means that the servocompensator is designed to be active only when the sliding surface variable ξ_c enters the boundary layer $\{|\xi_c| \le \mu\}$. Let ξ be the new sliding surface variable, which has the servocompensator part, such that

$$\hat{\xi} = K_\vartheta^T\vartheta + \hat{\xi}_c \tag{44}$$

where $\hat{\xi}$ and $\hat{\xi}_c$ are the surface functions constructed from estimated states. $\vartheta \in \mathcal{R}^m$ is the conditional servocompensator state vector. The conditional servocompensator dynamics are described as

$$\dot{\vartheta} = A_\vartheta\vartheta + \mu B_\vartheta \text{sat}(\hat{\xi}/\mu) \tag{45}$$

K_ϑ is a unique servomechanism gain vector, which will make the eigenvalues of matrix $(A_\vartheta + B_\vartheta K_\vartheta^T)$ equal to the eigenvalues of S, and the pair $(A_\vartheta, B_\vartheta)$ is chosen such that they are in controllable canonical form

$$A_\vartheta = \begin{bmatrix} 0 & 1 & 0 & \dots & 0 \\ 0 & 0 & 1 & \dots & 0 \\ \vdots & & & & \vdots \\ 0 & \dots & \dots & 0 & 1 \\ * & * & * & * & * \end{bmatrix}_{m\times m} \quad B_\vartheta = \begin{bmatrix} 0 \\ 0 \\ \vdots \\ 0 \\ * \end{bmatrix}_{m\times 1}$$

where the matrix A_ϑ is Hurwitz. Therefore, if $\vartheta(0)$ is $\mathcal{O}(\mu)$, $\vartheta(t)$ will be $\mathcal{O}(\mu)$ also.

To include the servomechanism in the control law, the switching control law u_w (38) is modified to

$$u_w = -\beta_w(t,e)\text{sat}\left(\frac{\hat{\xi}}{\mu}\right) \tag{46}$$

Let N be the solution of the following Sylvester equation:

$$NS - SN = -P^{-1}B_\vartheta(\Gamma + K_\vartheta^T PN)$$

It has been established in Ref. [63] that the existence and uniqueness of the solution N are ensured if A_ϑ and S have no common eigenvalues. In addition to that, if the pair $(A_\vartheta, B_\vartheta)$ is controllable and the pair (S, Γ) is observable, the matrix N is nonsingular [63]. The matrix P is a unique nonsingular similarity transformation matrix such that

$$P^{-1}(A_\vartheta + B_\vartheta K_\vartheta^T)P = S, \quad P^{-1}B_\vartheta = [0\,0\dots 0\,1]^T$$

If the eigenvalues of the exosystem (43) are unknown, due to the unknown frequencies of the inversion error $\delta_{\text{inv}}(t)$, it is needed to manipulate K_ϑ in Eq. (44) online with an adaptation law. Let $\hat{K}_\vartheta$ be the manipulated servomechanism gain vector. The adaptation law is designed to change the eigenvalues of the matrix $(A_\vartheta + B_\vartheta\hat{K}_\vartheta^T)$ online to become equal to the eigenvalues of S. To lower the number of adapted variables, we use the partial adaptation as suggested in Ref. [54], by defining the following vectors:

$$\lambda_\vartheta = \mathcal{I}_\vartheta K_\vartheta \quad \text{and} \quad v_\vartheta = \mathcal{I}_\vartheta\vartheta$$

where $\lambda_\vartheta \in \mathcal{R}^\imath$, $v_\vartheta \in \mathcal{R}_\imath$, and $\imath \le m$ is the number of the adapted variables, $\mathcal{I}_\vartheta$ is $(\imath \times m)$ matrix with its rows being unit vectors, and v_ϑ represents the adaptive regressor vector. As we mentioned above, the pair $(A_\vartheta, B_\vartheta)$ is in the controller canonical form, so the number of adaptation variables are

$$\imath = \begin{cases} \dfrac{m}{2}, & \text{if the number of frequencies is even} \\ \dfrac{m-1}{2}, & \text{if the number of frequencies is odd} \end{cases}$$

Assuming that λ_ϑ belongs to the convex hypercube $\varkappa_\vartheta = \{\lambda_\vartheta | a_i \le \lambda_{\vartheta_i} \le b_i, 1 \le i \le \imath\}$, then the adaptation law can be designed as

$$\begin{aligned}\dot{\hat{\lambda}}_\vartheta &= \beta_\vartheta(\hat{\xi},\mu)\mathcal{P}_r(\gamma_\vartheta(\hat{\xi}_c, v_\vartheta, \beta_w)) \text{ and} \\ \gamma_\vartheta(\hat{\xi}_c, v_\vartheta, \beta_w) &= \gamma_\vartheta\beta_w v_\vartheta(\mu_\vartheta \text{sat}(\hat{\xi}_c/\mu_\vartheta))/\mu^2\end{aligned} \tag{47}$$

where the function $\mathcal{P}_r(\cdot)$ is a parameter projection operator that retains $\hat{\lambda}_\vartheta$ in $\varkappa_\delta \supset \varkappa_\vartheta\, \forall t \ge 0$, where $\varkappa_\delta = \{\lambda_\vartheta | a_i - \delta \le \lambda_{\vartheta_i} \le b_i + \delta, 1 \le i \le \imath\}$, and $\delta > 0$. γ_ϑ is the adaptation gain and the parameter $0 < \mu_\vartheta < \mu$. The componentwise smooth projection $\mathcal{P}_r(\gamma_\vartheta(\hat{\xi}_c, v_\vartheta, \beta_w))$ is defined by

$$[\mathcal{P}_r(\gamma_\vartheta(\cdot))]_i = \begin{cases} \left(1 + \dfrac{b_i - \hat{\lambda}_{\vartheta_i}}{\delta}\right)\gamma_{\vartheta_i} & \text{if } \hat{\lambda}_{\vartheta_i} > b_i \text{ and } \gamma_{\vartheta_i} > 0 \\ \left(1 + \dfrac{\hat{\lambda}_{\vartheta_i} - a_i}{\delta}\right)\gamma_{\vartheta_i} & \text{if } \hat{\lambda}_{\vartheta_i} < a_i \text{ and } \gamma_{\vartheta_i} < 0 \\ \gamma_{\vartheta_i} & \text{Otherwise} \end{cases}$$

The function $\beta_\vartheta(\hat{\xi}, \mu)$ is defined as

$$\beta_\vartheta(\hat{\xi}, \mu) = \begin{cases} 0 & \text{if } |\hat{\xi}| \ge 2\mu \\ 1 & \text{if } |\hat{\xi}| \le \mu \\ 1 - \dfrac{|\hat{\xi}| - \mu}{\mu} & \text{if } \mu < |\hat{\xi}| < 2\mu \end{cases}$$

The purpose of the function $\beta_\vartheta(\hat{\xi}, \mu)$ is to keep $\hat{\lambda}_\vartheta$ constant outside the boundary set $\{|\hat{\xi}| \le 2\mu\}$.

Figure 5 provides a more comprehensive picture of the overall closed-loop system including the control law (36), the observer (42), and the adaptation law (47).

3.3 Output Feedback Closed-Loop System Dynamics.

The closed-loop dynamics under output feedback are composed of the exosystem dynamics (43), the conditional servomechanism (45), the semi-affine error dynamics (34), the adaptation law (47), the time-derivative of the modified sliding mode surface function (44), and the high-gain observer dynamics (42). By inserting the output feedback control law (36) into Eqs. (44) and (42) and then

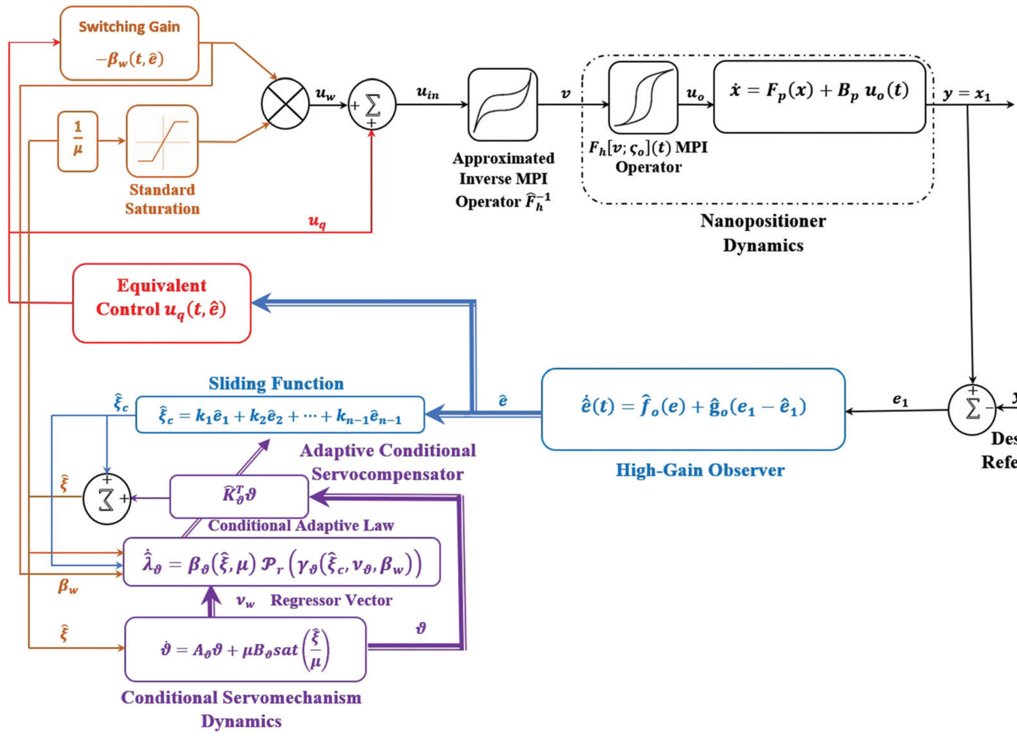

Fig. 5 Block diagram of the closed-loop system

doing algebraic manipulation, we can derive the closed-loop system in compact form as follows:

$$\dot{\mathcal{X}}(t) = \mathcal{F}_{\rm cl}(t,\mathcal{X},W_{\rm in}) = \bar{\mathcal{F}}_{\rm cl}(t,\mathcal{X}) + \varepsilon_h \mathcal{D}_{\rm inv}(\mathcal{X},W_{\rm in}) \tag{48}$$

where $\mathcal{F}_{\rm cl}$ is the closed-loop system under hysteresis inversion, $\bar{\mathcal{F}}_{\rm cl}$ is hysteresis-free closed-loop system ($\delta_{\rm inv}(t)=0$), $\mathcal{D}_{\rm inv}(\mathcal{X},W_{\rm in}) = \mathcal{B}_{\rm inv}W_{\rm in}(t)$, and these functions are defined as

$$\bar{\mathcal{F}}_{\rm cl}(t,\mathcal{X}) = \begin{bmatrix} S\omega \\ A_\vartheta\vartheta + \mu B_\vartheta {\rm sat}\left(\dfrac{\xi - L(\varepsilon)\phi}{\mu}\right) \\ A_\zeta\zeta + B_\zeta\left(\xi - \hat{K}_\vartheta^T\vartheta\right) \\ \Delta_{d_1}(\cdot) + \Delta_{d_2}(\cdot) - b\beta_w(t,\hat{e}){\rm sat}\left(\dfrac{\xi - L(\varepsilon)\phi}{\mu}\right) \\ \varepsilon^{-1}A_\phi\phi + B_\phi\left[-\delta_e(e) - b\beta_w(t,\hat{e}){\rm sat}\left(\dfrac{\xi - L(\varepsilon)\phi}{\mu}\right)\right] \\ \beta_\vartheta(\hat{\xi},\mu)\,\mathcal{P}_r\left(\gamma_\vartheta\left(\hat{\xi}_c, v_\vartheta, \beta_w\right)\right) \end{bmatrix}$$

$$\mathcal{B}_{\rm inv} = [0,0,0,b,b,0]^T$$

where $\mathcal{X} = [\omega,\vartheta,\zeta,\xi,\phi,\lambda_\vartheta]^T$, the pairs (A_ζ,B_ζ) and (A_φ,B_φ) are in the controller and observable canonical forms, respectively, and the matrices A_ζ and A_φ are Hurwitz. ϕ is the scaled estimation variable, which is defined as

$$\varphi_i = \frac{1}{\varepsilon^{n-i}}(e_i - \hat{e}_i)$$

The other terms and variables are defined as follows:

$$\begin{aligned} \Delta_{d_1}(\cdot) &= \hat{K}_\vartheta^T A_\vartheta\vartheta + \mu\hat{K}_\vartheta B_\vartheta {\rm sat}((\xi - L(\varepsilon)\varphi)/\mu) + \dot{\hat{\lambda}}_\vartheta v_\vartheta, \\ \Delta_{d_2}(\cdot) &= \sum_{n-1}^{i=1} k_i e_{i+1} - \delta_e(e), \\ \zeta^T &= [e_1\, e_2 \ldots e_{n-1}], \\ \phi^T &= [\phi_1\, \phi_2 \ldots \phi_n], \\ L(\varepsilon) &= [k_1\varepsilon^{n-1}\, k_2\varepsilon^{n-2}\, k_3\varepsilon^{n-3} \ldots k_{n-1}\varepsilon\, 1] \end{aligned}$$

Notice that the closed-loop system dynamics (48) include some nonlinearities, for example, the saturation function in the control law (38) and the projection function in adaptation control law (47). For the purpose of conducting the analysis in Sec. 4, the following assumption is needed. This is mainly due to the necessity to have a unique T-periodic solution for the hysteresis-free closed-loop system, which cannot be easily established for such nonlinear system. In addition to that, Lemma 1, in which the exponential stability of the hysteresis-free closed-loop system is established, is needed in Sec. 4 analysis (in particular, the proof of Theorem 2).

Assumption 6. *If the desired reference input y_d is T-periodic, then there exists a unique T-periodic solution $\mathcal{X}_T(t)$ for the hysteresis-free closed-loop system $\bar{\mathcal{F}}_{\rm cl}(t,\mathcal{X})$ in Eq. (48).*

Lemma 1. *(Exponential stability of the hysteresis-free closed-loop system) Let Assumptions 1–5 be satisfied. Consider the hysteresis-free closed-loop system*

$$\dot{\mathcal{X}}(t) = \bar{\mathcal{F}}_{\rm cl}(t,\mathcal{X}) \tag{49}$$

under ideal hysteresis inversion ($\delta_{\rm inv}(t)=0$). Let $\Omega_1 \subset \mathcal{R}$, $\Omega_2 \subset \mathcal{R}^n$, $\Omega_3 \subset \mathcal{R}^n$, and $\Omega_4 \subset \mathcal{R}^m$ be compact sets. Let $\vartheta(0) = \mathcal{O}(\mu)$ and ν_0 and $\hat{\zeta}(0)$ be bounded. Let the switching control under the hysteresis-free case be chosen as

$$u_w = -\beta_{w_{\max}}{\rm sat}\left(\frac{\xi}{\mu}\right)$$

where $\beta_{w_{\max}} = \max_{e\in\Omega_1,\, t\ge 0}\{\beta_w(t,e)\}$. Then there is $\mu^* > 0$ such that for every $\mu \in (0,\mu^*]$, there is $\varepsilon^* = \varepsilon^*(\mu) > 0$ such that for every $\mu \in (0,\mu^*]$ and $\varepsilon \in (0,\varepsilon^*]$ and for all initial conditions $\xi(0), e(0) \in \Omega_1 \times \Omega_2$, $\hat{e}(0) \in \Omega_3$, $\vartheta(0) \in \Omega^m$, $\hat{\lambda}_\vartheta \in \varkappa_\vartheta$, if $\bar{v}_\vartheta$ is persistently exciting, then the closed-loop variables vector $\mathcal{X}$ is bounded $\forall t \ge 0$ and the hysteresis-free closed-loop system $\bar{\mathcal{F}}_{\rm cl}(t,\mathcal{X})$ has an exponentially stable equilibrium point at $(e=0, \tilde{\vartheta}=0, \hat{e}=0, \tilde{\lambda}_\vartheta = 0)$, where $\tilde{\vartheta} = \vartheta - \bar{\vartheta}$, $\tilde{\lambda}_\vartheta = \hat{\lambda}_\vartheta - \lambda_\vartheta$, $\bar{v}_\vartheta$ is the regression vector, and $\bar{\vartheta}$ is the servocompensator state vector in the boundary-layer stage.

The proof of this lemma is carried out by repeating the steps of the proof of Theorem 1 in Ref. [54] for the hysteresis-free closed-loop system $\bar{\mathcal{F}}_{\mathrm{cl}}(t, \mathcal{X})$.

4 Well-Posedness and Periodic Stability of the Closed-Loop System With Hysteresis Inversion Perturbations

Before proving the existence of an exponentially stable, periodic solution of the closed-loop system dynamics under hysteresis inversion (48), we need to establish that the system (48) is well-posed. By establishing well-posedness, we mean establishing the existence and uniqueness of the solution of the closed-loop system (48).

THEOREM 1. *(Well-posedness of the hysteretic closed-loop system) Consider the closed-loop system under hysteretic inversion perturbation (48), and let $\Omega_{\mathcal{X}} \subset \mathcal{R}^{r_c}$ and $\Omega_{\mathcal{H}} \subset \mathbb{W}_t^{1,1}$ be compact sets and are defined as*

$$\Omega_{\mathcal{X}} := \{\mathcal{X} \in \mathcal{R}^{r_c} : ||\mathcal{X}(t) - \mathcal{X}(0)||_1 \le r_{\mathcal{X}}\}$$
$$\Omega_{\mathcal{H}} := \{W_{\mathrm{in}} \in \mathbb{W}_t^{1,1} : ||W_{\mathrm{in}}(t) - W_{\mathrm{in}}(0)||_{\mathbb{W}_t^{1,1}} \le r_{\mathcal{H}}\}$$

where $r_c = 2n + 2m + \imath$ and $r_{\mathcal{X}}, r_{\mathcal{H}} > 0$. Under the piecewise continuity of the function $\mathcal{F}_{\mathrm{cl}}(t, \mathcal{X}, W_{\mathrm{in}})$ in t and its local Lipschitz property in arguments $\mathcal{X}$ and W_{in}, such that the condition

$$\begin{aligned} &||\mathcal{F}_{\mathrm{cl}}(t, \mathcal{X}_1, W_{\mathrm{in}_1}) - \mathcal{F}_{\mathrm{cl}}(t, \mathcal{X}_2, W_{\mathrm{in}_2})||_1 \\ &\le L_\chi||\mathcal{X}_1(t) - \mathcal{X}_2(t)||_1 + L_W||W_{\mathrm{in}_1}(t) - W_{\mathrm{in}_2}(t)||_1 \end{aligned} \tag{50}$$

is satisfied for any $\mathcal{X}_1$, $\mathcal{X}_1 \in \Omega_{\mathcal{X}}$ and W_{in_1}, $W_{\mathrm{in}_2} \in \Omega_{\mathcal{H}}$ $\forall t \in [0, t_u]$, where $t_u > 0$. Then there exists $0 < t_c < t_u$, such that the system (48) has a unique solution $\mathcal{X}_T(t)$ for all $\mathcal{X}(0) \in \Omega_{\mathcal{X}}$ and $W_{\mathrm{in}}(0) \in \Omega_{\mathcal{H}}$ over the time interval $[0, t_c]$.

The proof of this theorem can be found in the Appendix. By establishing the well-posedness of the hysteretic closed-loop system (48), we are now prepared to prove its periodic stability. Define $u_{\mathrm{in}}^T = \alpha_{\mathrm{in}}(\mathcal{X}_T)$ and $v^T = F_h^{-1}[u_{\mathrm{in}}^T; \bar{x}_b(0)](t)$. Under Assumptions 1–6, u_{in}^T will be T-periodic and v^T will also be T-periodic, but after some transient period of time. To prove the existence of exponentially stable periodic solution of the hysteretic closed-loop system (48), we need to establish the existence of a contraction property for the composite hysteresis operator $\mathcal{W}_{\mathrm{in}}$ resulted from the inversion. This property can be established for a T-periodic reference input $y_d(t)$ if $u_{\mathrm{in}}(t)$ and $v(t)$ satisfy the following condition.

ASSUMPTION 7. *For any absolute continuous function v_c, define its oscillation within the time interval $[t_1, t_2]$ as*

$$\mathrm{osc}_{[t_1,t_2]}[v_c] = \sup_{t_1 \le \tau_1, \tau_2 \le t_2} |v_c(\tau_1) - v_c(\tau_2)|$$

Assume

$$\mathrm{osc}_{[0,T]}\left[\sum_{-l}^{l} \theta_{d_i}\mathcal{P}_{d_i}(u_{\mathrm{in}}^T)\right] > 2\bar{r}_{\max}$$
$$\text{and} \quad \mathrm{osc}_{[T,2T]}[v_T] > 2r_{\max}$$

where $r_{\max} = ||r||_\infty$ and $\bar{r}_{\max} = ||\bar{r}||_\infty$.

THEOREM 2. *(Periodic stability of the hysteretic closed-loop system) Consider the hysteretic closed-loop system (48). Let Assumptions 1–7 be satisfied and let $\bar{\Omega}_{\mathcal{X}} \subset \mathcal{R}^{r_c}$ and $\bar{\Omega}_{\mathcal{H}} \subset \mathbb{W}_t^{1,1}$ be compact sets. Assume $\Delta_0 < 1$. Under T-periodic desired reference $y_d(t)$ and under the exponential stability of the hysteretic-free closed-loop system (49), there exists $\varepsilon_h^* \le \varepsilon_{h_{\max}}$, such that for all the initial conditions $\mathcal{X}(0) \in \bar{\Omega}_{\mathcal{X}}$ and $W_{\mathrm{in}}(0) \in \bar{\Omega}_{\mathcal{H}}$, the solution $\mathcal{X}(t)$ of the hysteretic closed-loop system (48) will converge exponentially to a unique periodic solution $\mathcal{X}_T(t)$.*

Proof. Consider the ith backlash operator $\mathcal{P}_{b_i}$ with radius r_i in Eq. (7), for the input $u_{\mathrm{in}}(t)$ with $\mathrm{osc}_{[0,T]} > 2r_i$ and two different initial conditions $\mathcal{X}_{b_i}^a(0)$ and $\mathcal{X}_{b_i}^b(0)$. It can be seen that the backlash operator $\mathcal{P}_{b_i}$ has the following property:

$$|\mathcal{P}_{b_i}[u_{\mathrm{in}}; \mathcal{X}_{b_i}^a(0)](t) - \mathcal{P}_{b_i}[u_{\mathrm{in}}; \mathcal{X}_{b_i}^b(0)](t)| = 0, \ \forall t > T \tag{51}$$

This mainly follows from the essential properties of the backlash operator (7), where its output oscillation becomes independent of the initial condition once its input oscillation amplitude exceeds $2r_i$. Refer to the composite MPI operator $\mathcal{W}_{\mathrm{in}}$ in Eq. (33) resulting from the inversion process. This operator is a composition of the inverse MPI operator F_h^{-1} (whose largest radius is $\bar{r}_{\max}$) and the MPI operator F_h (whose largest radius is $r_{\max}$). Using the property (51) and Assumption 7, we can show that the operator $\mathcal{W}_{\mathrm{in}}$ obeys the following contraction property:

$$|\mathcal{W}_{\mathrm{in}}[u_{\mathrm{in}}; x_{\mathrm{inv}}^a(0)](t) - \mathcal{W}_{\mathrm{in}}[u_{\mathrm{in}}; x_{\mathrm{inv}}^b(0)](t)| = 0 \ \ \forall t > 2T \tag{52}$$

where $x_{\mathrm{inv}}^a(0)$ and $x_{\mathrm{inv}}^b(0)$ are two different applicable initial inputs. Notice that even if $\mathcal{W}_{\mathrm{in}}$ operator includes deadzone nonlinearities, we still can establish the contraction property (52). This is because the deadzone nonlinearity is memory-less and preserves the local Lipschitz property. Similarly, by using the property (52) along with Assumption 7, we can show that the shift operator $\mathrm{Sh}^{\varepsilon_h}$ defined as

$$\mathrm{Sh}^{\varepsilon_h} : (\mathcal{X}(0), W_{\mathrm{in}}(0)) \to (\mathcal{X}(2T), W_{\mathrm{in}}(2T)) \tag{53}$$

has a contraction property for $\varepsilon_h > 0$. Since the MPI operator $\mathcal{W}_{\mathrm{in}}$ satisfies both the Volterra and semigroup properties [64], also from Proposition 1, we can show that

$$|W_{\mathrm{in}}(t)| \le \bar{\Delta}_0|\mathcal{X}(t)| + \bar{\Delta}_1$$

where $\bar{\Delta}_0$ and $\bar{\Delta}_1$ are positive constants and are function of the constants Δ_0 and Δ_1 of inequality (23). From Lemma 1, under the persistency of excitation of the regressor vector $\bar{\nu}_\vartheta$, we can show that the hysteresis-free closed-loop system (49) is T-convergent about $\mathcal{X}_T$ [51]. From Theorem 1, we have established the existence and uniqueness (well-posedness) of the solution of the hysteretic closed-loop system (48). Therefore, by following similar steps to those of Theorem (2.1) of Ref. [51], we can establish that the solution of the hysteretic closed-loop system (48) will converge exponentially to a unique periodic solution when ε_h is sufficiently small. ∎

In Theorem 2, we have established that the solution of the closed-loop system converges exponentially to a periodic solution provided the inversion error is sufficiently small. Furthermore, it can be shown that an ultimate bound on the tracking error can be reduced by reducing the controller parameters μ and ε. The ultimate boundedness can be established by following similar steps in the proofs of Theorems 1 and 2 of Ref. [53]. The first step is to show that the closed-loop systems variables in the reaching phase will converge exponentially to a positively invariant set that is parameterized by the parameters (μ and ε), which can shrink to zero if these two parameters are pushed to zero. The second step is to establish that the closed-loop system variables in the boundary-layer phase are ultimately bounded by a bound that depends on the controller parameters (μ and ε) and the inversion error perturbation $\varepsilon_h\mathcal{D}_{\mathrm{inv}}(\mathcal{X}, W_{\mathrm{in}})$.

5 Experimental Results

In this section, we examine the performance of the proposed control scheme by implementing tracking experiments on a commercial piezo-actuated nanopositioner stage (Nano-OP65) shown in Fig. 6. This platform, manufactured by Mad City Labs Inc., provides a practical tool to benchmark our controller in handling hysteretic disturbances. Position measurement is provided by a built-in capacitive sensor, where the travel range of the

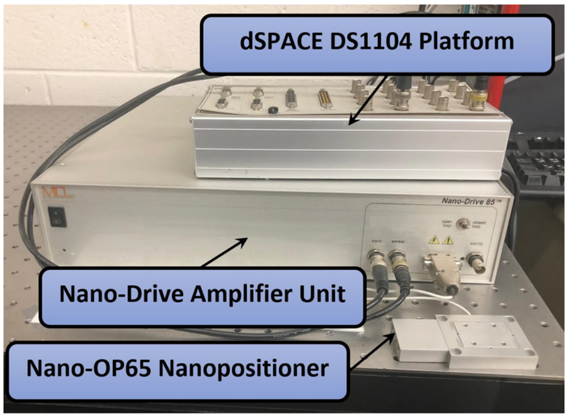

(*a*)

(*b*)

Fig. 6 Experimental setup of the nanopositioner system. (a) The complete setup including the nanopositioner stage Nano-OP65, Nano-Drive power amplifier unit, and the dSPACE DS1104 data acquisition interface unit and (b) magnified picture of the nanopositioner stage Nano-OP65.

nanopositioner is $\pm 65\ \mu$m. The power amplifier unit (Nano-Drive, Mad City Labs, Inc., Madison, WI) drives the piezo actuator and has a gain of 15. In the system setup, the manipulated control input is the one to the power amplifier not the actual voltage input to the piezo actuator. For real-time implementation, the controller is deployed to dSPACE (DS1104) platform using MATLAB/SIMULINK real-time coder tools.

The nanopositioner system is modeled with a second-order system in the form of Eq. (1). Due to the asymmetric hysteresis characteristics exhibited by the system, the hysteresis part is modeled with an MPI operator with eight play operators and nine deadzone operators, and the weights and thresholds are identified as [65]

$$\begin{aligned}
\hat{\theta}_b^T &= [0.719, 0.183, 0.035, 0.055, 0.034, 0.033, 0.023, 0.061] \\
r^T &= [0, 0.33, 0.66, 1.00, 1.33, 1.66, 2.00, 2.33] \\
\hat{\theta}_d^T &= [1.062, 0.473, 0.641, 0.311, 8.426, -0.636, -0.501, -0.614, -0.415] \\
d^T &= [-2.68, -1.97, -1.22, -0.42, 0, 0.32, 1.02, 1.76, 2.57]
\end{aligned}$$

The linear part of the model is identified using frequency-based identification methods, and its parameters are found to be $a_1 = -1.795 \times 10^8$, $a_2 = -5696.88$, and $b = 1.063 \times 10^9$ [65]. The identified model is found well-representative of the system behavior with the first resonant frequency of 1.227×10^4 rad/s and bandwidth of 2.0147×10^4 rad/s. Note that due to the high resonant frequency of the system, the identified parameters are very large.

The high-gain observer (42) is implemented with the gains h_1 and h_2 being 3 and 20, respectively. The parameter ε is taken as 0.0001. For the parameters of the switching function $\beta_w(\cdot)$ in Eq. (46), we calculate first the constants Δ_0 and Δ_1 of the bound (23) by using the formulas (24) and (25). From the identified weights and thresholds of the MPI hysteresis model mentioned above, we calculate the following:

$$||\hat{\theta}_b||_\infty = 0.719, \quad ||\hat{\theta}_d||_\infty = 8.426, \quad \text{and} \quad ||r||_\infty = 2.33$$

Then, we use the procedure provided in Ref. [50] to calculate the inverse MPI operator parameters, and accordingly we find

$$\sum_{i=0}^{7} |\bar{\theta}_{bi}| = 1.9082, \quad \sum_{j=-4}^{4} |\bar{\theta}_{dj}| = 0.187, \quad \text{and} \quad ||\bar{r}||_\infty = 2.2379$$

To ensure periodic stability, one major assumption of Theorem 2 is $\Delta_0 < 1$. To comply with this assumption, let $\varepsilon_{h_{\max}} = 0.015$, then by using formulas (24) and (25), the error bound (23) constants can be computed as $\Delta_0 = 0.9058$ and $\Delta_1 = 0.049$. The rest of the switching function (41) parameters are chosen as $\Gamma_1 = \Gamma_2 = 10$. We chose the sliding function (35) constant $k_1 = 5000$ and the boundary-layer width constant $\mu = 1000$. The boundary-layer width μ is chosen by gradually reducing it until we reach a point where the surface function starts to chatter. We then take a value above this threshold to maintain the device safety. Notice that the high-gain observer parameter ε is chosen smaller than the parameter μ such that the high-gain observer is the fastest portion of the dynamics.

For the adaptive servocompensator, we assume that the residual disturbance in the boundary-layer phase (due to hysteresis inversion) has only in its frequency spectrum the fundamental frequency of the desired reference input. Moreover, we assume that there is an additional bias disturbance term alongside the periodic disturbance terms. As a result, the internal model will be a third-order model (namely, a second-order model augmented with an integrator state).

To ensure the robustness of the adaptation law (47) against noise inputs and the observer peaking effect, the adaptation parameter λ_ϑ is assumed to be retained in the following convex set:

$$\varkappa_\delta = \{\lambda_\vartheta | -8.1 \leq \lambda_\vartheta \leq 8.1\}$$

The remaining adaptation law parameters are chosen as $\gamma_\vartheta = 2.68 \times 10^5$ and $\mu_\vartheta = 1$. The selection of the adaptation gain γ_ϑ is done by gradually increasing it until it is noticed that increasing the gains will not enhance the adaptation performance. In the adaptation law (47), we added the function $(\mu_\vartheta \text{sat}(\tilde{\xi}_c/\mu_\vartheta))$ due to the benefit seen in the experimental implementation of the controller for enhancing the adaptation performance and reducing the measurement noise effect; however, in the original approach of Ref. [54], it is not mandatory. The parameter μ_ϑ is selected by gradually reducing its value until no further enhancement in the adaptation performance is achieved. In our experiments, we test the proposed controller using three types of desired reference signals. The first one is a sinusoidal input defined as

$$y_d(t) = 10 \sin(2\pi f t) + 10\ \mu\text{m}$$

with frequency $f = 5$, 25, 50, and 100 Hz. It is worth mentioning that we published part of our evaluation results using sinusoidal reference in Ref. [52]. Therefore, we are not going to repeat these results in this paper. In Tables 1 and 2, we conduct a comparison

Table 1 Percentage of mean tracking error (mean $|e(t)|$%) with respect to the maximum peak-to-peak value of the reference under sinusoidal reference input for the proposed controller versus competing methods

Frequency (Hz)	SMC	SHSC	MHSC	EHGO–DI	PI	Inv-B ACS
5	0.0595	0.3245	0.1355	0.0672	0.0736	0.0016
25	0.3100	0.3535	0.1340	0.0665	0.0939	0.0041
50	0.3300	0.3850	0.1420	0.0686	0.1498	0.0101
100	0.4150	0.4075	0.1760	0.1026	0.2897	0.0148

Table 2 Percentage of peak tracking error (max $|e(t)|\%$) with respect to the maximum peak-to-peak value of the reference under sinusoidal reference input for the proposed controller versus competing methods

Frequency (Hz)	SMC	SHSC	MHSC	EHGO–DI	PI	Inv-B ACS
5	0.4750	0.8600	0.4495	0.1153	0.7894	0.0083
25	0.8500	0.9250	0.4405	0.1383	0.8422	0.0212
50	1.1250	0.9650	0.5050	0.1821	1.0058	0.0465
100	1.3750	1.1900	0.7850	0.3333	1.5185	0.0610

between the achieved tracking error accuracy of our proposed approach in the boundary-layer phase as compared to other control approaches proposed in previous projects implemented on the same experimental setup. Those approaches are (a) the inversion-based sliding mode controller proposed in Ref. [34] and it will be abbreviated as SMC, (b) the results of Ref. [29], in which both of SHSC and MHSC are designed and implemented, (c) the results obtained from combining extended high-gain observer and the dynamic inversion (EHGO–DI) approaches, which appear in Ref. [49], and (d) a classical PI controller without hysteresis inversion implemented experimentally by the authors and its gains are chosen to yield the best possible performance.

In Tables 1 and 2, we show the percentage of the maximum absolute tracking error and the percentage of the mean absolute tracking error with respect to the maximum peak-to-peak value of the reference. It can be noticed in both tables that the inversion-based adaptive conditional servocompensator (Inv-B ACS) approach greatly outperforms the other five approaches in reducing the tracking errors for all frequencies. The trend in both tables shows that the next best tracking performance comes from the approach using the EHGO–DI. Note that the mean absolute error for the EHGO–DI approach is higher than the Inv-B ACS one by almost sevenfolds for the 100 Hz frequency.

The second round of experiments are done using a sawtooth desired reference with the same frequencies used with the sinusoidal reference (frequencies 5, 25, 50, and 100 Hz). A second-order prefilter is inserted to smooth out the signal to avoid spiking impulses at the signal edges. The measured output displacement $y(t)$ under the inversion-based ACS control method for the 100 Hz frequency reference case is shown in Fig. 7. In Fig. 8, the tracking error $e_1(t)$ is presented. The magnified subfigure to the left side shows the tracking error response for the first 0.03 s. Notice that the tracking error converges quickly in around 0.003 s. Another magnified subfigure added to the right shows a time interval of the tracking error in the boundary-layer phase (7.0–7.1 s). Notice that the error is not increasing in the period (0.03–10 s).

In Fig. 9, we show the frequency spectral content of the tracking error in the boundary-layer phase (0.03–10 s) for the 100 Hz reference. It is noticed that we have nine harmonics shown in the

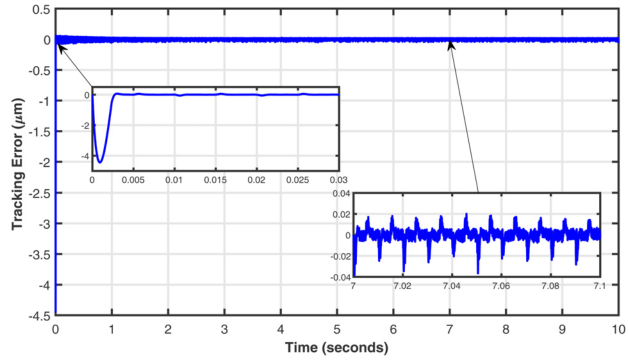

Fig. 8 Tracking error with a sawtooth reference with 100 Hz frequency

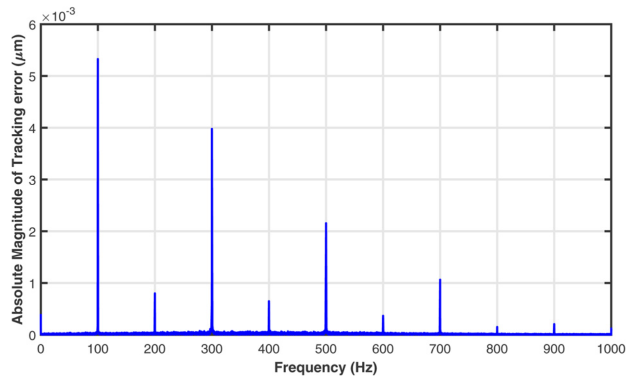

Fig. 9 Frequency spectrum of the tracking error with a 100 Hz sawtooth reference in the boundary-layer phase

spectrum with odd harmonics being relatively stronger than the even harmonics, which are barely noticeable. It can be seen that the first harmonic (the fundamental) has magnitude of less than 5.5 nm, and the rest of harmonics are lower than this magnitude.

Another set of experiments are conducted using the van der Pol oscillator output as desired reference input to the system. In Fig. 10, the measured output displacement $y(t)$ is shown for the 100 Hz frequency. In Fig. 11, we demonstrate the tracking error $e(t)$ performance. Similar to the sawtooth reference case, it can be noticed that the tracking error converges around 0.003 s. However, the tracking error magnitudes are a little bit higher than those in the sawtooth reference case. This can be seen clearly in Fig. 12, in which we demonstrate the spectrum content of the tracking error frequency. It can be seen that the fundamental harmonic has magnitude of 14 nm as compared to less than 5.5 nm in the sawtooth

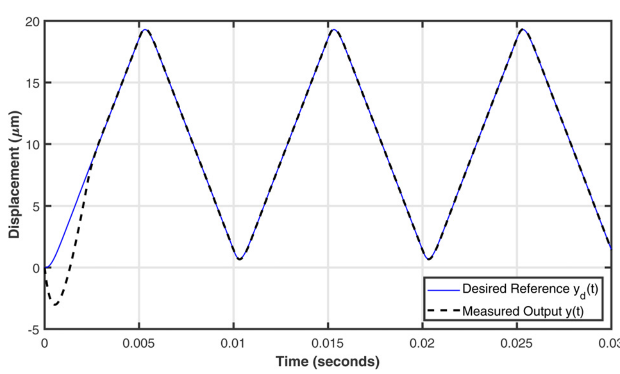

Fig. 7 Measured displacement versus sawtooth desired reference with 100 Hz frequency using the inversion-based ACS

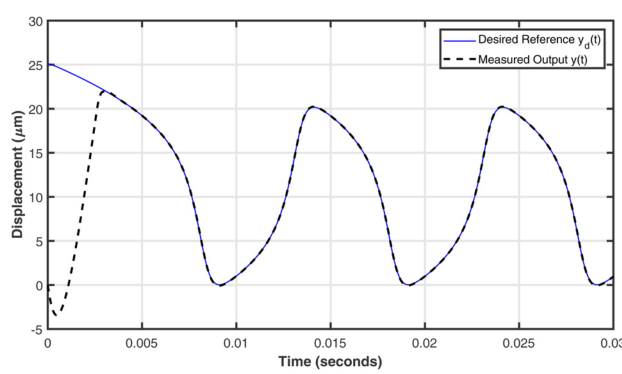

Fig. 10 Measured displacement versus van der Pol desired reference with 100 Hz frequency using the inversion-based ACS

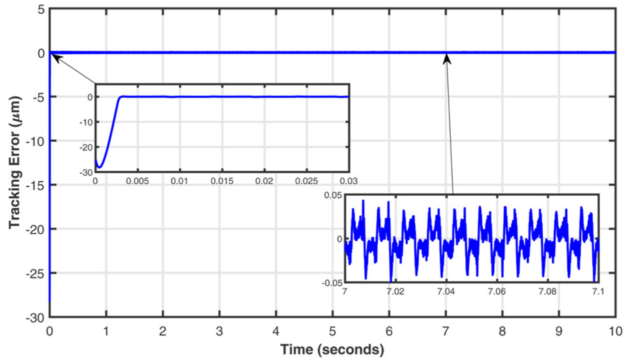

Fig. 11 Tracking error with a van der Pol reference with 100 Hz frequency

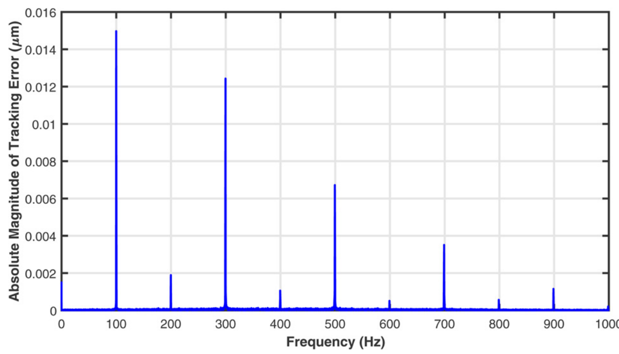

Fig. 12 Frequency spectrum of the tracking error with a 100 Hz van der Pol reference in the boundary-layer phase

reference case. We can see in Fig. 12 that we have nine harmonics in the signal spectrum similar to the sawtooth reference, but with higher amplitudes.

Finally, in Table 3, we offer a comparison in absolute percentage tracking errors for the sawtooth and van der Pol references' cases. It can be observed in the table that for all the tested frequencies, the van der Pol reference case has higher tracking errors as compared to the sawtooth case. For instant, in the 100 Hz frequency case, we can see that the mean absolute error in the van der Pol reference case is larger by more than three times compared to the sawtooth reference case. This is an indication that the van der Pol reference stimulates strongly the disturbance odd harmonics as compared to the previous two references.

Notice that we have done the same set of experiments to the controller of Ref. [53], and the tracking error results came comparable to this work. The tracking errors of this controller can be made smaller if a more accurate hysteresis model is used.

It is worth mentioning that we tried replacing the switching function designed based on the analytical error bound by a constant gain taken as the maximum of the switching function $\beta_w(\cdot)$ for $t \geq 0$. However, the results obtained from the fixed switching gain have shown that the tracking errors have increased with more aggressive control actions for all the considered references.

Table 3 Percentage of tracking errors for the proposed controller with respect to the reference maximum peak under sawtooth and van der Pol desired references

	Sawtooth		van der Pol	
Frequency (Hz)	Mean $\vert e(t)\vert$%	Max $\vert e(t)\vert$%	Mean $\vert e(t)\vert$%	Max $\vert e(t)\vert$%
5	0.0016	0.0133	0.0017	0.0210
25	0.0054	0.0481	0.0075	0.0560
50	0.0104	0.1027	0.0202	0.1291
100	0.0226	0.2584	0.0707	0.3695

In the implementation of the adaptive servocompensator (45), to avoid the case when the matrix S has very large eigenvalues, we utilized the technique suggested in Ref. [66] to scale down the internal model matrices such that $A_\vartheta = g_\vartheta \bar{A}_\vartheta$ and $B_\vartheta = g_\vartheta \bar{B}_\vartheta$, where $\bar{A}_\vartheta$ is chosen as a Hurwitz matrix with eigenvalues $(-1, -1.5, -2)$ and the pair $(\bar{A}_\vartheta, \bar{B}_\vartheta)$ is in controllable canonical form, g_ϑ is the scaling factor and is chosen to be $2\pi \times 600$. This technique helps in making the adaptation parameters in K_ϑ reasonably small.

6 Conclusion

This paper focuses on designing an adaptive conditional servocompensator for a class of hysteretic systems. Under this control law, the behavior of the closed-loop system has two stages. The first one is a reaching phase, where the controller is a continuously implemented sliding mode control law. For this stage, we have designed the control law to accommodate hysteric inversion error perturbations by deriving an analytical bound on these perturbations, which is used to design the switching control component. Then, we designed the switching part of the control law using the analytical bound to reduce the conservativeness of the sliding mode controller. The second stage starts when the sliding variable enters the boundary layer and stays therein forever. In particular, at this time, the adaptation law is activated "conditionally" to handle the residual hysteretic perturbations.

Aside from the proposed new control algorithms with experimentally proven performance, this work makes contributions to the theory of systems with hysteresis. Our stability analysis embodied in Theorems 1 and 2 establishes well-posedness and periodic stability for the closed-loop system. The theoretical framework used to prove the periodic stability was originally presented in Ref. [51]; however, some of the assumptions in Ref. [51] are not satisfied due to nonsmooth terms in both the control and the adaptation laws. In our work, we have been able to establish the periodic stability of the closed-loop system under mild conditions. Experimental validation of our proposed control algorithm, including both advanced inversion-based and inversion-free algorithms and the traditional PI controller, confirms its superiority as compared with competing control algorithms implemented on the same device. We note that the proposed control algorithm is computationally efficient, as it does not involve solving sophisticated optimization problems or require online estimation of hysteresis parameters.

Funding Data

- National Science Foundation (CMMI 1301243, Funder ID: 10.13039/100000001).

Appendix: Proof of Theorem 1

Define the following integration operator:

$$\mathcal{X}(t) := \mathcal{C}[\mathcal{X}](t) = \mathcal{X}^o + \int_0^t \mathcal{F}_{\text{cl}}(s, \mathcal{X}, \mathcal{W}_{\text{inv}}[u_{\text{in}}; W_{\text{in}}(0)](s))\text{d}s \tag{A1}$$

where $\mathcal{X}^o = \mathcal{X}(0)$ and the mapping $\mathcal{C}[\mathcal{X}](t) : \Omega_\mathcal{X} \times \Omega_\mathcal{H} \to \Omega_\mathcal{X} \times \Omega_\mathcal{H}$. Due to the equivalence of solutions of both Eqs. (48) and (A1), we will continue the proof using Eq. (A1). Let us define a closed set $\mathcal{S} \subset [0, t] \times \mathcal{R}^{r_c} \times \mathbb{W}_t^{1,1}$

$$\mathcal{S} := \{t \in [0, t_c],\ \mathcal{X} \in \Omega_\mathcal{X}, \quad \text{and} \quad W_{\text{in}} \in \Omega_\mathcal{H}\}$$

where $t_c > 0$ will be calculated shortly. The first step in order to establish that $\mathcal{C}[\mathcal{X}](t)$ is a contraction over $\mathcal{S}$ is to show that $\mathcal{C}[\mathcal{X}](t)$ maps $\mathcal{S}$ into itself. To do this, we rewrite Eq. (A1) by adding and subtracting the term $\mathcal{F}_{\text{cl}}(s, \mathcal{X}^o, \mathcal{W}_{\text{inv}}[u^o_{\text{in}}; W_{\text{in}}(0)](s))$ inside the integral

$$\mathcal{C}[\mathcal{X}](t) - \mathcal{X}^o = \int_0^t [\mathcal{F}_{\rm cl}(s, \mathcal{X}, \mathcal{W}_{\rm inv}[u_{\rm in}; W_{\rm in}(0)](s)) + \mathcal{F}_{\rm cl}(s, \mathcal{X}^o, \mathcal{W}_{\rm inv}[u^o_{\rm in}; W_{\rm in}(0)](s)) - \mathcal{F}_{\rm cl}(s, \mathcal{X}^o, \mathcal{W}_{\rm inv}[u^o_{\rm in}; W_{\rm in}(0)](s))]{\rm d}s \quad \text{(A2)}$$

where $u^o_{\rm in}$ is the control input evaluated at $t=0$. From the local Lipschitz continuity properties of the function $\mathcal{F}_{\rm cl}(\cdot)$, the function $\mathcal{F}_{\rm cl}(t, \mathcal{X}, \mathcal{W}_{\rm inv}[u^o_{\rm in}; W_{\rm in}(0)](t))$ is bounded over the interval $t \in [0, t_u]$, and for all $\mathcal{X}, W_{\rm in} \in S$, where the final value of t_c will be picked later no greater than t_u. Hence, define

$$b_f \triangleq \max_{\mathcal{X}, W_{\rm in} \in \mathcal{S}^{t \in [0,t_u]}} ||\mathcal{F}_{\rm cl}\left(t, \mathcal{X}^o, \mathcal{W}_{\rm inv}[u^o_{\rm in}; W_{\rm in}(0)](t)\right)||_1$$

From the Lipschitz properties of the function $\mathcal{F}_{\rm cl}(\cdot)$ and in light of the definition of the standard norm (13), we can show that the first two terms of the integrand in Eq. (A2) satisfy the following inequality:

$$||\mathcal{F}_{\rm cl}(s, \mathcal{X}, \mathcal{W}_{\rm inv}[u_{\rm in}; W_{\rm in}(0)](s)) - \mathcal{F}_{\rm cl}(s, \mathcal{X}^o, \mathcal{W}_{\rm inv}[u^o_{\rm in}; W_{\rm in}(0)](s))||_1 \leq L_{x_1}||\mathcal{X} - \mathcal{X}^o|||_{\mathbb{W}_t^{1,1}} + L_{h_1}||\mathcal{W}_{\rm inv}[u_{\rm in}; W_{\rm in}(0)](s) - \mathcal{W}_{\rm inv}[u^o_{\rm in}; W_{\rm in}(0)](s)||_{\mathbb{W}_t^{1,1}} \quad \text{(A3)}$$

where L_{x_1} and L_{h_1} are the corresponding Lipschitz constants dependent on $\mathcal{X}^o$, $r_\mathcal{X}$, and $r_\mathcal{H}$. By using the Lipschitz property of the MPI operator $\mathcal{W}_{\rm inv}[\cdot]$, proven in Proposition 1, we have

$$||\mathcal{W}_{\rm inv}[u_{\rm in}; W_{\rm in}(0)](s) - \mathcal{W}_{\rm inv}[u^o_{\rm in}; W_{\rm in}(0)](s)||_{\mathbb{W}_t^{1,1}} \leq L_{h_2}||u_{\rm in} - u^o_{\rm in}||_{\mathbb{W}_t^{1,1}}$$

Let $u_{\rm in}(t) = \alpha_{\rm in}(.)$, where $\alpha_{\rm in}(.)$ is a piecewise continuous function in t, then inside the set $\mathcal{S}$, we can derive

$$\begin{aligned} ||u_{\rm in} - u^o_{\rm in}||_{\mathbb{W}_t^{1,1}} &= \int_0^t ||u'_{\rm in}(s) - u^{o\prime}_{\rm in}(s)||_1 {\rm d}s \leq \int_0^t \left|\left|\frac{\partial\alpha_{\rm in}(\mathcal{X})}{\partial\mathcal{X}}\mathcal{X}'\right|\right|_1 \\ &\leq \int_0^t \left|\left|\frac{\partial\alpha_{\rm in}(\mathcal{X})}{\partial\mathcal{X}}\right|\right|_1 ||\mathcal{X}'||_1 \leq \int_0^t c_1||\mathcal{X}'(s)||_1{\rm d}s \\ &\leq c_1 r_\mathcal{X} \end{aligned} \quad \text{(A4)}$$

where

$$c_1 = \max_{\mathcal{X}\in\mathcal{S}} \left|\left|\frac{\partial\alpha_{\rm in}(\mathcal{X})}{\partial\mathcal{X}}\right|\right|_1 \quad \text{(A5)}$$

Notice that the norm $||\cdot||_1$ in Eq. (A5) is an induced norm. Now taking the 1-norm of both sides of Eq. (A2), and utilizing the local Lipschitz properties of $\mathcal{F}_{\rm cl}(\cdot)$ along with inequalities (A3) and (A4), we get

$$||\mathcal{C}[\mathcal{X}](t) - \mathcal{X}^o||_1 \leq ||\mathcal{C}[\mathcal{X}](t) - \mathcal{X}^o||_{\mathbb{W}t^{1,1}} \leq \int_0^t [L_{x_1}||\mathcal{X}(s) - \mathcal{X}^o(s)||_{\mathbb{W}t^{1,1}} + L_{h_1}||\mathcal{W}_{\rm inv}[u_{\rm in}; W_{\rm in}(0)](s) - \mathcal{W}_{\rm inv}[u^o_{\rm in}; W_{\rm in}(0)](s)||_{\mathbb{W}t^{1,1}} + b_f]{\rm d}s \leq t_c b_q \quad \text{(A6)}$$

where $b_q = L_{x_1}r_\mathcal{X} + L_{h_1}L_{h_2}c_1r_\mathcal{X} + b_f$. From the above inequality, we have established the boundedness of the function $\mathcal{F}_{\rm cl}(s, \mathcal{X}, \mathcal{W}_{\rm inv}[u_{\rm in}; W_{\rm in}(0)](s))$. Hence, by choosing $t_c \leq r_\mathcal{X}/b_q$, we can ensure that $\mathcal{C}[\mathcal{X}](t) : \mathcal{S} \to \mathcal{S}$.

The next step is to show that the mapping $\mathcal{C}[\mathcal{X}](t)$, with careful selection of t_c, is a contraction mapping over $\mathcal{S}$. Let $\mathcal{X}_1$ and $\mathcal{X}_2 \in \mathcal{S}$, and consider the norm

$$\begin{aligned} ||\mathcal{C}[\mathcal{X}_1](t) - \mathcal{C}[\mathcal{X}_2](t)||_1 &= \int_0^t ||\mathcal{F}_{\rm cl}(s, \mathcal{X}_1, \mathcal{W}_{\rm inv}[u^1_{\rm in}; W_{\rm in}(0)](s)) \\ &- \mathcal{F}_{\rm cl}(s, \mathcal{X}_2, \mathcal{W}_{\rm inv}[u^2_{\rm in}; W_{\rm in}(0)](s))||_1{\rm d}s \leq \int_0^t [L_{x_1}||\mathcal{X}_1(s) - \mathcal{X}_2(s)||_{\mathbb{W}t^{1,1}} \\ &+ L_{h_1}||\mathcal{W}_{\rm inv}[u^1_{\rm in}; W_{\rm in}(0)](s) - \mathcal{W}_{\rm inv}[u^2_{\rm in}; W_{\rm in}(0)](s)||_{\mathbb{W}t^{1,1}}]{\rm d}s \\ &\leq t_c[L_{x_1}||\mathcal{X}_1(s) - \mathcal{X}_2(s)||_{\mathbb{W}t^{1,1}} + L_{h_1}L_{h_2}||u^1_{\rm in} - u^2_{\rm in}||_{\mathbb{W}t^{1,1}}] \end{aligned} \quad \text{(A7)}$$

Similar to the steps that lead to Eq. (A4), we have

$$\begin{aligned} ||u^1_{\rm in}(s) - u^2_{\rm in}(s)||_{\mathbb{W}_t^{1,1}} &= \int_0^t ||u^{1\prime}_{\rm in}(s) - u^{2\prime}_{\rm in}(s)||_1{\rm d}s \\ &\leq \int_0^t \left[\left|\left|\frac{\partial\alpha_{\rm in}(\mathcal{X}_1(s))}{\partial\mathcal{X}}\mathcal{X}'_1(s) - \frac{\partial\alpha_{\rm in}(\mathcal{X}_2(s))}{\partial\mathcal{X}}\mathcal{X}'_2(s)\right|\right|_1{\rm d}s\right. \end{aligned} \quad \text{(A8)}$$

By adding and subtracting the term $(((\partial\alpha_{\rm in}(\mathcal{X}_1(s)))/\partial\mathcal{X})\mathcal{X}'_2(s))$, inside the norm of the above integral, we have

$$\begin{aligned} ||u^1_{\rm in}(s) - u^2_{\rm in}(s)||_{\mathbb{W}_t^{1,1}} &\leq \int_0^t || \frac{\partial\alpha_{\rm in}(\mathcal{X}(s))}{\partial\mathcal{X}}[\mathcal{X}'_1(S) - \mathcal{X}'_2(S)] \\ &- \left[\frac{\partial\alpha_{\rm in}(\mathcal{X}_1(s))}{\partial\mathcal{X}} - \frac{\partial\alpha_{\rm in}(\mathcal{X}_2(s))}{\partial\mathcal{X}}\right]\mathcal{X}'_2(s)||_1{\rm d}s \\ &\leq \int_0^t \left[c_1||\mathcal{X}'_1(s) - \mathcal{X}'_2(s)||_{\mathbb{W}_t^{1,1}} + L_{\alpha_{\rm in}}||\mathcal{X}_2||_{\mathbb{W}_t^{1,1}} \max_{\mathcal{X}\in\mathcal{S}} ||\mathcal{X}_1(s) - \mathcal{X}_2||_{\mathbb{W}_t^{1,1}}\right]{\rm d}s \\ &\leq b_\rho||\mathcal{X}_1(s) - \mathcal{X}_2||_{\mathbb{W}_t^{1,1}} \end{aligned} \quad \text{(A9)}$$

where $b_\rho = c_1 + c_2L_{\alpha_{\rm in}}$, $c_2 = \max_{\mathcal{X}\in\mathcal{S}}||\mathcal{X}_2||_{\mathbb{W}_t^{1,1}}$, and $L_{\alpha_{\rm in}}$ is the local Lipschitz constant of the function $\partial\alpha_{\rm in}/\partial\mathcal{X}$, which is dependent on the constants $r_\mathcal{X}$ and t_c. By combining inequalities (A8) and (A9), with inequality (A7), we get

$$||\mathcal{C}[\mathcal{X}_1](t) - \mathcal{C}[\mathcal{X}_2](t)||_{\mathbb{W}_t^{1,1}} \leq t_c\rho_\mathcal{X}||\mathcal{X}_1(t) - \mathcal{X}_2(t)||_{\mathbb{W}_t^{1,1}} \quad \text{(A10)}$$

where $\rho_\mathcal{X} = L_{x_1} + L_{h_1}L_{h_2}b_\rho$. Therefore, by taking $t_c \leq \rho_c/\rho_\mathcal{X}$, for any $0 \leq \rho_c \leq 1$, we have

$$||\mathcal{C}[\mathcal{X}_1](t) - \mathcal{C}[\mathcal{X}_2](t)||_{\mathbb{W}_t^{1,1}} \leq \rho_c||\mathcal{X}_1(t) - \mathcal{X}_2(t)||_{\mathbb{W}_t^{1,1}}$$

which implies that $\mathcal{C}[\mathcal{X}](t)$ is a contraction mapping over the set $\mathcal{S}$. Combining all the previous analysis, and by using the contraction mapping Theorem (B.1) of Ref. [60], we conclude that if

$$t_c \leq \min\left\{\left\{t_u, \frac{r_\mathcal{X}}{b_q}, \frac{\rho_c}{\rho_\mathcal{X}}\right\}\right.$$

then there is a unique solution $\mathcal{X}(t) \in \mathcal{S}$ that satisfies Eq. (A1), for all $t \leq t_c$. With that, we have established the uniqueness of the solution of Eq. (A1) in the set $\mathcal{S}$. We need to show the uniqueness of the solution in $\mathbb{W}_t^{1,1}$. We can prove that by showing that for any $\mathcal{X}_o \in \Omega_\mathcal{X}$, the solution cannot leave the set $\Omega_\mathcal{X}$. To see this, let the time t_p be such that the solution $\mathcal{X}(t_p)$ leaves the boundary of the set $\Omega_\mathcal{X}$. By following similar steps that led to Eq. (A6), we get

$$r_\mathcal{X} = ||\mathcal{X}(t_p) - \mathcal{X}_o||_1 \leq t_pb_q \Rightarrow t_p \geq \frac{r_\mathcal{X}}{b_q} \Rightarrow t_p \geq t_c$$

which means that $\mathcal{X}(t)$ cannot leave the set $\Omega_\mathcal{X}$ for all time $t \leq t_c$, and this implies that any solution $\mathcal{X}(t) \in \mathbb{W}_t^{1,1}$ lies in $\mathcal{S}$, from which the uniqueness of the solution is established in the space $\mathbb{W}_t^{1,1}$.

References

[1] Hou, J., Liu, L., Wang, Z., Wang, Z., Xi, N., Wang, Y., Wu, C., Dong, Z., and Yuan, S., 2013, "AFM-Based Robotic Nano-Hand for Stable Manipulation at Nanoscale," IEEE Trans. Autom. Sci. Eng., **10**(2), pp. 285–295.

[2] Tuma, T., Sebastian, A., Lygeros, J., and Pantazi, A., 2013, "The Four Pillars of Nanopositioning for Scanning Probe Microscopy: The Position Sensor, the Scanning Device, the Feedback Controller, and the Reference Trajectory," IEEE Control Syst. Mag., **33**(6), pp. 68–85.

[3] Bhagat, U., Shirinzadeh, B., Tian, Y., and Zhang, D., 2013, "Experimental Analysis of Laser Interferometry-Based Robust Motion Tracking Control of a Flexure-Based Mechanism," IEEE Trans. Autom. Sci. Eng., **10**(2), pp. 267–275.

[4] Lai, L.-J., Gu, G.-Y., and Zhu, L.-M., 2012, "Design and Control of a Decoupled Two Degree of Freedom Translational Parallel Micro-Positioning Stage," Rev. Sci. Instrum., **83**(4), p. 045105.

[5] Tian, Y., Zhang, D., and Shirinzadeh, B., 2011, "Dynamic Modelling of a Flexure-Based Mechanism for Ultra-Precision Grinding Operation," Precis. Eng., **35**(4), pp. 554–565.
[6] Gozen, B. A., and Ozdoganlar, O. B., 2012, "Design and Evaluation of a Mechanical Nanomanufacturing System for Nanomilling," Precis. Eng., **36**(1), pp. 19–30.
[7] Lai, L.-J., Zhou, H., Du, Y.-J., Zhang, J., Jia, J.-C., Jiang, L.-M., Zhu, L.-M., Tian, Z.-W., Tian, Z.-Q., and Zhan, D.-P., 2013, "High Precision Electrochemical Micromachining Based on Confined Etchant Layer Technique," Electrochem. Commun., **28**, pp. 135–138.
[8] Tseng, A. A., 2011, "Advancements and Challenges in Development of Atomic Force Microscopy for Nanofabrication," Nano Today, **6**(5), pp. 493–509.
[9] Casuso, I., Khao, J., Chami, M., Paul-Gilloteaux, P., Husain, M., Duneau, J.-P., Stahlberg, H., Sturgis, J. N., and Scheuring, S., 2012, "Characterization of the Motion of Membrane Proteins Using High-Speed Atomic Force Microscopy," Nat. Nanotechnol., **7**(8), pp. 525–529.
[10] Müller, D. J., Krieg, M., Alsteens, D., and Dufrêne, Y. F., 2009, "New Frontiers in Atomic Force Microscopy: Analyzing Interactions From Single-Molecules to Cells," Curr. Opin. Biotechnol., **20**(1), pp. 4–13.
[11] Gu, G., Zhu, L., Su, C., and Ding, H., 2013, "Motion Control of Piezoelectric Positioning Stages: Modeling, Controller Design, and Experimental Evaluation," IEEE/ASME Trans. Mechatron., **18**(5), pp. 1459–1471.
[12] Rakotondrabe, M., 2013, *Smart Materials-Based Actuators at the Micro/Nano-Scale: Characterization, Control and Applications*, Springer-Verlag, New York.
[13] Tao, G., and Kokotovic, P. V., 1995, "Adaptive Control of Plants With Unknown Hystereses," IEEE Trans. Autom. Control, **40**(2), pp. 200–212.
[14] Lee, J., Jin, M., Kashiri, N., Caldwell, D. G., and Tsagarakis, N. G., 2019, "Inversion-Free Force Tracking Control of Piezoelectric Actuators Using Fast Finite-Time Integral Terminal Sliding-Mode," Mechatronics, **57**, pp. 39–50.
[15] Adriaens, H. J. M. T. S., De Koning, W. L., and Banning, R., 2000, "ModelingPiezoelectric Actuators," IEEE/ASME Trans. Mechatron., **5**(4), pp. 331–341.
[16] Liu, Y., Liu, H., Wu, H., and Zou, D., 2016, "Modelling and Compensation of Hysteresis in Piezoelectric Actuators Based on Maxwell Approach," Electron. Lett., **52**(3), pp. 188–190.
[17] Wang, D., Zhu, W., and Yang, Q., 2011, "Linearization of Stack Piezoelectric Ceramic Actuators Based on Bouc-Wen Model," J. Intell. Mater. Syst. Struct., **22**(5), pp. 401–413.
[18] Chen, Y., Qiu, J., Palacios, J., and Smith, E. C., 2013, "Tracking Control of Piezoelectric Stack Actuator Using Modified Prandtl–Ishlinskii Model," J. Intell. Mater. Syst. Struct., **24**(6), pp. 753–760.
[19] Croft, D., Shed, G., and Devasia, S., 2001, "Creep, Hysteresis, and Vibration Compensation for Piezoactuators: Atomic Force Microscopy Application," ASME J. Dyn. Syst., Meas., Control, **123**(1), pp. 35–43.
[20] Song, G., Zhao, J., Zhou, X., and Abreu-Garcia, J. A. D., 2005, "Tracking Control of a Piezoceramic Actuator With Hysteresis Compensation Using Inverse Preisach Model," IEEE/ASME Trans. Mechatron., **10**(2), pp. 198–209.
[21] Al Janaideh, M., and Krejci, P., 2013, "Inverse Rate-Dependent Prandtl–Ishlinskii Model for Feedforward Compensation of Hysteresis in a Piezomicropositioning Actuator," IEEE/ASME Trans. Mechatron., **18**(5), pp. 1498–1507.
[22] Janaideh, M. A., Rakotondrabe, M., Al-Darabsah, I., and Aljanaideh, O., 2018, "Internal Model-Based Feedback Control Design for Inversion-Free Feedforward Rate-Dependent Hysteresis Compensation of Piezoelectric Cantilever Actuator," Control Eng. Pract., **72**, pp. 29–41.
[23] Edardar, M., Tan, X., and Khalil, H. K., 2014, "Tracking Error Analysis for Feedback Systems With Hysteresis Inversion and Fast Linear Dynamics," ASME J. Dyn. Syst., Meas., Control, **136**(4), p. 041010.
[24] Schitter, G., Stemmer, A., and Allgower, F., 2003, "Robust 2 DOF-Control of a Piezoelectric Tube Scanner for High Speed Atomic Force Microscopy," Proceedings of the 2003 American Control Conference, Vol. 5, Denver, CO, June 4–6, pp. 3720–3725.
[25] Al Janaideh, M., Rakotondrabe, M., and Aljanaideh, O., 2016, "Further Results on Hysteresis Compensation of Smart Micropositioning Systems With the Inverse Prandtl–Ishlinskii Compensator," IEEE Trans. Control Syst. Technol., **24**(2), pp. 428–439.
[26] Yan, Y., Wang, H., and Zou, Q., 2012, "A Decoupled Inversion-Based Iterative Control Approach to Multi-Axis Precision Positioning: 3D Nanopositioning Example," Automatica, **48**(1), pp. 167–176.
[27] Wang, Z., and Zou, Q., 2015, "A Modeling-Free Differential-Inversion-Based Iterative Control Approach to Simultaneous Hysteresis-Dynamics Compensation: High-Speed Large-Range Motion Tracking Example," 2015 American Control Conference (ACC), Chicago, IL, July 1–3, pp. 3558–3563.
[28] Tan, X., and Khalil, H. K., 2009, "Two-Time-Scale Averaging of Systems Involving Operators and Its Application to Adaptive Control of Hysteretic Systems," 2009 American Control Conference, St. Louis, MO, June 10–12, pp. 4476–4481.
[29] Esbrook, A., Tan, X., and Khalil, H. K., 2013, "Control of Systems With Hysteresis Via Servocompensation and Its Application to Nanopositioning," IEEE Trans. Control Syst. Technol., **21**(3), pp. 725–738.
[30] Esbrook, A., Tan, X., and Khalil, H. K., 2013, "An Indirect Adaptive Servocompensator for Signals of Unknown Frequencies With Application to Nanopositioning," Automatica, **49**(7), pp. 2006–2016.
[31] Bashash, S., and Jalili, N., 2007, "Robust Multiple Frequency Trajectory Tracking Control of Piezoelectrically Driven Micro/Nanopositioning Systems," IEEE Trans. Control Syst. Technol., **15**(5), pp. 867–878.
[32] Cao, Y., and Chen, X. B., 2012, "Integrated Inversion-Feedforward and PID-Based-Sliding-Mode-Control for Piezoelectric Actuators," 2012 American Control Conference (ACC), Montreal, QC, June 27–29, pp. 869–874.
[33] McMahan, J. A., and Smith, R. C., 2012, "Sliding Mode Control Based on an Inverse Compensator Design for Hysteretic Smart Systems," 2012 IEEE 51st IEEE Conference on Decision and Control (CDC), Maui, HI, Dec. 10–13, pp. 985–990.
[34] Edardar, M., Tan, X., and Khalil, H. K., 2015, "Design and Analysis of Sliding Mode Controller Under Approximate Hysteresis Compensation," IEEE Trans. Control Syst. Technol., **23**(2), pp. 598–608.
[35] Ghafarirad, H., Rezaei, S. M., Abdullah, A., Zareinejad, M., and Saadat, M., 2011, "Observer-Based Sliding Mode Control With Adaptive Perturbation Estimation for Micropositioning Actuators," Precis. Eng., **35**(2), pp. 271–281.
[36] Qiao, Z., Gan, M., and Wang, C., 2014, "Sliding Mode Control Using Linear Extended State Observer (LESO) and Hysteresis Compensator Based on Bouc-Wen Model in Sinusoidal Position Control of a Piezoelectric Actuator," Proceedings of the 33rd Chinese Control Conference, Nanjing, China, July 28–30, pp. 3840–3845.
[37] Xu, R., and Zhou, M., 2017, "Integral Sliding Mode Tracking Control of Piezoelectric Positioning Platform With Compensating Hysteresis-Observer," 2017 International Conference on Advanced Mechatronic Systems (ICAMechS), Xiamen, China, Dec. 6–9, pp. 472–476.
[38] Xu, R., Zhang, X., Guo, H., and Zhou, M., 2018, "Sliding Mode Tracking Control With Perturbation Estimation for Hysteresis Nonlinearity of Piezo-Actuated Stages," IEEE Access, **6**, pp. 30617–30629.
[39] El-Shaer, A. H., Janaideh, M. A., Krejčí, P., and Tomizuka, M., 2013, "Robust Performance Enhancement Using Disturbance Observers for Hysteresis Compensation Based on Generalized Prandtl–Ishlinskii Model," ASME J. Dyn. Syst., Meas., Control, **135**(5), p. 051008.
[40] Feng, Z., Ling, J., Ming, M., and Xiao, X., 2019, "Integrated Modified Repetitive Control With Disturbance Observer of Piezoelectric Nanopositioning Stages for High-Speed and Precision Motion," ASME J. Dyn. Syst., Meas., Control, **141**(8), p. 081006.
[41] Chen, X., Hisayama, T., and Su, C.-Y., 2009, "Pseudo-Inverse-Based Adaptive Control for Uncertain Discrete Time Systems Preceded by Hysteresis," Automatica, **45**(2), pp. 469–476.
[42] Chen, X., Hisayama, T., and Su, C., 2010, "Adaptive Control for Uncertain Continuous-Time Systems Using Implicit Inversion of Prandtl-Ishlinskii Hysteresis Representation," IEEE Trans. Autom. Control, **55**(10), pp. 2357–2363.
[43] Sofla, M. S., Rezaei, S. M., Zareinejad, M., and Saadat, M., 2010, "Hysteresis-Observer Based Robust Tracking Control of Piezoelectric Actuators," Proceedings of the 2010 American Control Conference, Baltimore, MD, June 30–July 2, pp. 4187–4192.
[44] Chen, J., Ren, B., and Zhong, Q. C., 2015, "Hysteresis Compensation in Piezoelectric Actuator Positioning Control Based on the Uncertainty and Disturbance Estimator," 2015 American Control Conference (ACC), Chicago, IL, July 1–3, pp. 2537–2542.
[45] Nie, Z., Ma, Y., Wang, Q., Guo, D., and Liu, R., 2016, "Model Reference Compensation for Hysteresis System Based on Extended State Observer," 2016 35th Chinese Control Conference (CCC), Chengdu, China, July 27–29, pp. 757–762.
[46] Wei, W., Xia, P., Xue, W., and Zuo, M., 2020, "On the Disturbance Rejection of a Piezoelectric Driven Nanopositioning System," IEEE Access, **8**, pp. 74771–74781.
[47] Janaideh, M. A., and Boker, A. M., 2018, "Modeling and Output-Feedback Control of Systems With Netushil Rate-Dependent Hysteresis Nonlinearties," 2018 IEEE Conference on Decision and Control (CDC), Miami, FL, Dec. 17–19, pp. 6912–6917.
[48] Chowdhury, D., Al-Nadawi, Y. K., and Tan, X., 2018, "Hysteresis Compensation Using Extended High-Gain Observer and Dynamic Inversion," ASME Paper No. DSCC2018-9082.
[49] Chowdhury, D., Al-Nadawi, Y. K., and Tan, X., "Dynamic Inversion-Based Hysteresis Compensation Using Extended High-Gain Observer," Automatica (under review).
[50] Kuhnen, K., 2003, "Modeling, Identification and Compensation of Complex Hysteretic Nonlinearities: A Modified Prandtl-Ishlinskii Approach," Eur. J. Control, **9**(4), pp. 407–418.
[51] Brokate, M., and Pokrovskiı, A., 1998, "Asymptotically Stable Oscillations in Systems With Hysteresis Nonlinearities," J. Differ. Equations, **150**(1), pp. 98–123.
[52] Al-Nadawi, Y. K., Tan, X., and Khalil, H. K., 2017, "An Adaptive Conditional Servocompensator Design for Nanopositioning Control," 56th IEEE Annual Conference on Decision and Control (CDC 2017), Melbourne, Australia, Dec. 12–15, pp. 885–890.
[53] Al-Nadawi, Y. K., Tan, X., and Khalil, H. K., 2021, "Inversion-Free Hysteresis Compensation Via Adaptive Conditional Servomechanism With Application to Nanopositioning Control," IEEE Trans. Control Syst. Technol., **29**(5), pp. 1922–1935.
[54] Li, R., and Khalil, H. K., 2012, "Nonlinear Output Regulation With Adaptive Conditional Servocompensator," Automatica, **48**(10), pp. 2550–2559.
[55] Krasnosel'skii, M. A., and Pokrovskii, A. V., 1989, *Systems With Hysteresis*, Springer Verlag, Berlin.
[56] Iyer, R. V., and Tan, X., 2009, "Control of Hysteretic Systems Through Inverse Compensation," IEEE Control Syst. Mag., **29**(1), pp. 83–99.
[57] Janaideh, M. A., Rakheja, S., and Su, C.-Y., 2009, "A Generalized Prandtl-Ishlinskii Model for Characterizing the Hysteresis and Saturation Nonlinearities of Smart Actuators," Smart Mater. Struct., **18**(4), p. 045001.
[58] Kuhnen, K., and Janocha, H., 1999, "Adaptive Inverse Control of Piezoelectric Actuators With Hysteresis Operators," 1999 European Control Conference (ECC), Karlsruhe, Germany, Aug. 31–Sept. 3, pp. 791–796.

[59] Krejcí, P., and Kuhnen, K., 2008, "Existence, Uniqueness and L_∞-Stability of the Prandtl-Ishlinskii Hysteresis and Creep Compensator," Eur. J. Control, **14**(5), pp. 409–417.
[60] Khalil, H. K., 2002, *Nonlinear Systems*, 3rd ed., Prentice Hall, Upper Saddle River, NJ.
[61] Khalil, H., 2017, *High-Gain Observers in Nonlinear Feedback Control*, Society for Industrial and Applied Mathematics, Philadelphia, PA.
[62] Esfandiari, F., and Khalil, H. K., 1992, "Output Feedback Stabilization of Fully Linearizable Systems," Int. J. Control, **56**(5), pp. 1007–1037.
[63] Nikiforov, V., 1998, "Adaptive Non-Linear Tracking With Complete Compensation of Unknown Disturbances," Eur. J. Control, **4**(2), pp. 132–139.
[64] Brokate, M., and Sprekels, J., 1996, *Hysteresis and Phase Transitions*, Springer-Verlag, New York.
[65] Esbrook, A. J., 2012, "Control of Systems With Hysteresis Using Servocompensators," Ph.D. thesis, Michigan State University, East Lansing, MI.
[66] Serrani, A., Isidori, A., and Marconi, L., 2001, "Semi-Global Nonlinear Output Regulation With Adaptive Internal Model," IEEE Trans. Autom. Control, **46**(8), pp. 1178–1194.